2011-01-01

Preparation of Tissues and Cells for Infrared and Raman Spectroscopy and Imaging

Fiona Lyng
Technological University Dublin, Fiona.lyng@tudublin.ie

Ehsan Gazi

Peter Gardner

Section 2
Technical Aspects

CHAPTER 5

Preparation of Tissues and Cells for Infrared and Raman Spectroscopy and Imaging

FIONA LYNG,[a] EHSAN GAZI[b] AND PETER GARDNER[b]

[a] Radiation and Environmental Science Centre, Focas Institute, Dublin Institute of Technology, Kevin St, Dublin 8, IRELAND; [b] School of Chemical Engineering and Analytical Science, Manchester Interdisciplinary Biocentre, University of Manchester, 131 Princess Street, Manchester, M1 7DN, UK

5.1 Introduction

Fourier transform infrared (FTIR) and Raman spectroscopy can provide important structural information on the molecular composition of a sample as well as relative quantification of lipids, proteins, carbohydrates and a variety of phosphorylated biomolecules within cells or tissue. However, sample preparation is the key to realizing the full potential of these technologies. This element of the experimental design can have a significant impact on the interpretation of spectra for their biochemical relevance and on the spatial distribution of biomolecules in imaging studies.

This chapter contains two main parts, the first part (section 5.2) deals with sample preparation for tissues, and the second part (section 5.3) deals with sample preparation for cells. In section 5.2, tissue preparation methods for spectroscopic analysis such as cryopreservation (section 5.2.2), fixation (section 5.2.3) and embedding (section 5.2.4) are described and a number of studies investigating the

RSC Analytical Spectroscopy Monographs No. 11
Biomedical Applications of Synchrotron Infrared Microspectroscopy
Edited by David Moss

Published by the Royal Society of Chemistry, www.rsc.org

effects of these tissue processing steps are presented and discussed. In section 5.3, cell preparation methods such as drying and fixation (section 5.3.2) are described and again studies investigating the effects of these processing steps are discussed. Cell preparation methods for biomechanistic studies (section 5.3.3) and the effects of cell culture growth media and substrates on spectroscopic analysis of cells (section 5.3.4) are also included in this section. The preparation of live cells for FTIR and Raman spectroscopy (section 5.3.5) is also discussed.

5.2 Tissue Preparation

5.2.1 Introduction to Tissue Preparation Methods

Surgically excised tissue may undergo one of two commonly used methods of preservation for long-term storage: paraffin embedding or flash-freezing. The choice between these two methods is based on the specific purpose of the resected tissue.

Currently, formalin fixation and paraffin preservation (FFPP) is the preferred source for the histological examination of tissue sections. This method involves immersing tissue in an aqueous formalin solution. Hydrated formalin (methylene glycol, OH–CH–OH) is a coagulative protein fixative, which cross-links the primary and secondary amine groups of proteins,[1] but preserves some lipids by reacting with the double bonds of unsaturated hydrocarbon chains.[2] Following formalin fixation, the tissue is dehydrated through consecutive immersions in increasing grades of ethanol up to 100% ethanol. Displacement of water with ethanol preserves the secondary structure of proteins but denatures their tertiary structure. Furthermore, formalin or ethanol induces coagulation of the globular proteins present in the cytoplasm, which can result in the loss of structural integrity of organelles such as mitochondria. Another disadvantage is that ethanol precipitates lipid molecules that are not preserved through the primary fixation step. However, stabilization of intercellular proteins by formalin and ethanol localizes associated glycogen. Following dehydration, the alcohol is replaced by an organic solvent such as xylene, which is miscible with both alcohol and molten paraffin wax. The tissue is then immersed in and permeated by molten paraffin wax. The infiltration of the wax into the intracellular spaces is promoted by the previous ethanol dehydration step that created pores in the plasma membrane of the cells. The tissue sample is then cooled to room temperature, which solidifies the wax. This process provides a physical support to the sample enabling thin sections (usually 2–7 μm) to be cut without deformation to the cellular structure or architecture.

Snap-freezing of fresh tissue is generally preferred for molecular based studies since this method avoids the use of organic solvents that cause degradation or loss of some cellular components. In particular, frozen sections are used to study enzymes and soluble lipids. Furthermore, this method is used to conduct immunohistochemical analysis since some antigens may be affected by extensive cross-linking chemical fixatives that denature their tertiary structure.

In the case of snap-freezing, the water contained within the cells acts as the supporting medium. Fresh tissue is snap-frozen in liquid nitrogen cooled isopentane ($-170\,^{\circ}C$) to promote vitreous ice formation and to prevent ice crystal damage, since the latter can produce holes in the tissue and destroy cellular morphology and tissue architecture. The hardened tissue can then be embedded in mounting medium such as OCT (optimal cutting temperature compound) for sectioning within a cryostat maintained at $-17\,^{\circ}C$ and then subsequently stained.

Optimal cutting temperature compound is a viscous solution at room temperature, consisting of a resin–polyvinyl alcohol, an antifungal agent, benzalkonium chloride and polyethylene glycol to lower the freezing temperature.[3] Turbett *et al.* suggested that snap-frozen tissues should be stored without any medium since it was found that amplification of deoxyribonucleic acid (DNA), extracted from these tissues, was significantly affected for segments of greater than 300 base-pairs.[3] However, ribonucleic acid (RNA) was found to be unaffected.

Although the methods outlined above represent the gold standard tissue processing techniques in most pathology laboratories, some researchers have recently reported alternative tissue preparation protocols with the view of optimizing the assessment of specific biomolecular domains. Gillespie *et al.* conducted a comparative molecular profiling study in clinical tissue specimens that were fixed for long-term storage with widely used techniques (snap-frozen and formalin fixed paraffin embedded) and a less common method of 70% ethanol fixation and paraffin embedding.[4] The researchers found that although the total protein quantity was decreased in fixed and embedded tissues compared to snap frozen tissue, two-dimensional polyacrylamide gel electrophoresis (2D-PAGE) analysis of proteins from ethanol-fixed, paraffin-embedded prostate shared 98% identity with a matched sample from the same patient that was snap-frozen. This indicated that the molecular weights and isoelectric points of the proteins were not disturbed by the tissue processing method. The general quality and the quantity of the proteins in the ethanol-fixed samples were found to be superior to formalin-fixed tissue. Furthermore, Gillespie *et al.* reported that recovery of messenger RNA (mRNA) and DNA was more pronounced in ethanol-fixed specimens compared with formalin-fixed samples.[4] Thus, further improvements to tissue processing methodologies will play a key role in ultimately determining the complete molecular anatomy of normal and diseased human cell types.

Researchers working in the field of FTIR and Raman tissue diagnostics have employed a variety of methods for tissue preparation. Early FTIR spectroscopic studies have been carried out using ground samples of snap-frozen tissue for the bulk analysis of chemical composition.[5,6] Using this method, Andrus *et al.* reported an increasing ratio of peak areas corresponding to bands at $1121\,cm^{-1}$ and $1020\,cm^{-1}$ (attributed to RNA/DNA), which were associated with increased aggressiveness of malignant non-Hodgkin's lymphomas.[5] Takahashi *et al.* used bulk tissue analysis to study glycogen levels in tissues obtained from colorectal tumours, regions adjacent to the tumour and regions

of normal colorectum.[6] The results indicated that there was a statistically significant difference in glycogen levels (peak area ratio $1045\,cm^{-1}/1545\,cm^{-1}$) between cancer tissue and the other two regions.[6]

The use of ground tissue provides indiscriminate and composite measurement of both epithelial and stromal tissue compartments. However, care must be taken with this type of analysis when molecular assignments are made for discriminatory bands. In the study by Andrus *et al.*, the influence of collagen absorbance was discussed.[5] However, other confounding variables exist in stromal tissue, namely a variety of cell types such as endothelial cells of blood vessels, fibroblasts, ganglia and erythrocytes, in addition to possible bisecting nerves and muscle. This was clearly demonstrated by Fernandez *et al.* who classified several prostate tissue components for diagnostic FTIR imaging.[7]

A number of papers have been published that compare the effects of different sample preparation protocols for FTIR and Raman microspectroscopic studies,[8–11] and these are discussed in the following sections.

5.2.2 Fresh and Cryopreserved Tissue

More than a decade ago, Shim and Wilson[8] demonstrated that dehydration at room temperature of fresh tissue specimens (subcutaneous fat, smooth muscle, cheek pouch epithelium, oesophagus) resulted in Raman spectra with a decrease in intensity of the $930\,cm^{-1}$ (C–C stretch of proline and valine) peak relative to the peaks at $1655\,cm^{-1}$ and $1450\,cm^{-1}$. Although this may be indicative of protein denaturing, the authors did not observe any shifts in the amide I peak. However, an increase in the lipid:protein signal was observed with increasing drying times, providing evidence that the protein vibrational modes were perturbed by dehydration. Interestingly, Shim and Wilson found that Raman spectra obtained from OCT-freeze stored, snap-frozen tissue in phosphate buffered saline (PBS) were comparable to spectra obtained from fresh tissue in PBS.[8] Additional peaks observed at lower frequency ($764\,cm^{-1}$ and $795\,cm^{-1}$) in the spectra of snap-frozen adipose tissue were attributed to the coagulation of erythrocytes.

AQ1

Faoláin *et al.* also conducted a comparative study of frozen and fresh tissue using parenchymal tissue from the placenta (Figure 5.1).[9] Here, the authors did find significant differences in the Raman spectra, a reduction in the intensity of bands at $1002\,cm^{-1}$ (C–C aromatic ring stretching), $1447\,cm^{-1}$ (CH_2 bending mode of proteins and lipids) and $1637\,cm^{-1}$ (Amide I band of proteins) in the frozen tissue compared with fresh tissue. Additionally, frozen tissue exhibited a new peak at $1493\,cm^{-1}$, which was not found to be OCT contamination but was attributed to an artefact of the freezing process. It was suggested that this artefact was due to depolymerization of the actin cytoskeleton, resulting in an increased contribution of the NH_3^+ deformation mode.[9] Using FTIR microspectroscopy, the frozen tissue was found to display an overall reduction in intensity, while shifts in the Amide I and II bands indicated changes in protein conformation in the frozen tissue section.[9]

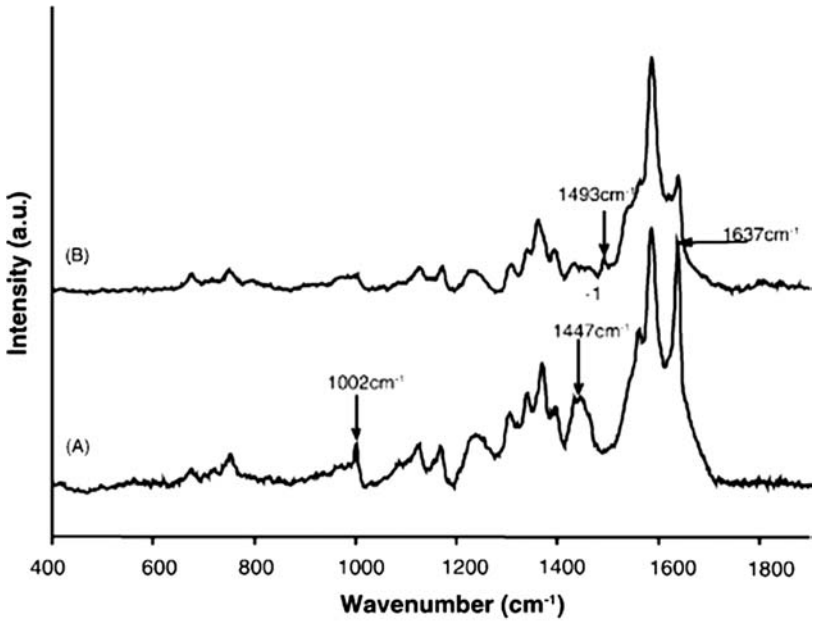

Figure 5.1 Raman spectra of (A) fresh tissue compared with (B) frozen tissue section. (Reproduced from reference [9].)

AQ2

AQ1

It is important to note that in the study by Faoláin *et al.*,[9] the comparison of fresh and frozen tissue was carried out with prior mounting onto MirrIR slides on which the frozen tissue had been thawed before analysis. Hence, depolymerization of proteins can also result from post-thawing of the frozen tissue, whereby the undesirable transition of vitreous ice into ice crystals could affect the integrity of the cytoskeletal proteins. It is well known within the structural cell biology community that this can be prevented by the application of freeze-drying. However, Shim and Wilson's investigations suggest that the spectral changes in protein vibrational modes, caused by heat induced denaturing of thawed frozen tissue, can be circumvented by thawing in PBS (maintained at room temperature).[8] Another molecular change associated with tissue thawing and dehydration was found to include a change in the relative intensities of the Amide I and methyl bending modes.[8]

The extent of protein depolymerization that has been observed in Raman spectra of freeze-dried tissue can be reduced by using an appropriate cryogen for the initial snap-freezing of the resected tissue specimen. Higher freezing rates are achieved using propane or mixtures of propane and isopentane in preference to isopentane.[12] Also, since ice crystals develop in a temperature range of 0 to $-140\,^{\circ}C$,[12] it is advantageous to maintain cryopreserved tissues at temperatures lower than $-140\,^{\circ}C$ during microtomy and freeze-drying. Finally, the size of the specimen also dictates the extent of ice crystal damage; in liquid nitrogen cooled propane, it has been reported that $0.5\,mm^3$ is the critical

size that separates complete crystallization from partial vitrification.[12] Nevertheless, Stone *et al.* have demonstrated on a number of different tissue types that freeze-thawed tissue, without PBS, can be used to differentiate different pathologies with greater than 90% sensitivity and specificity.[13] The same method of sample preparation was used to demonstrate the biochemical basis for tumour progression of prostate and bladder cancers by determining the relative amounts of a number of tissue constituents.[14] This was carried out by obtaining Raman spectra of pure standards and correlating these with tissue spectra derived from each disease state using ordinary least-squares analysis. The biological explanations for these constituent changes through the different pathological states could be associated with known tumour behaviour. Thus, freeze–thawed tissue warmed to room temperature is not only diagnostically useful but may also provide relative quantifications and qualitative biomolecular characterization of the sample.

Recently, Wills *et al.* compared cryopreserved (banked) tissue with fresh tissue using Raman spectroscopy and found a high correlation, suggesting that frozen tissue from tissue banks could be used to develop diagnostic algorithms for use with fresh tissue samples.[15]

For FTIR investigations, snap-frozen tissue has been analysed following thawing and subsequent air-drying to avoid interference from water bands.[16–19] However, this dehydration process can result in undesirable perturbations to cellular chemistry, and some researchers have reported using cryosections dried under a stream of nitrogen gas to reduce oxidative and surface tension effects [20, 21].[20,21] Both protocols have successfully been applied to the spectral classification of tissue pathologies,[16–21] and have been shown to generate detailed biospectroscopic maps that localize tumour lesions within oral[20] and brain tissues.[21] Additionally, using a univariate analytical approach to process tissue maps, Wiens *et al.* reported the use of dried snap-frozen sections to investigate the early appearance and development of scar tissue using FTIR signals corresponding to lipids, sugars and phosphates as well as collagen and its fibril orientation.[19]

5.2.3 Chemical Fixation of Tissue

It is important to note that the process of fixation is not instantaneous and two important properties of the fixative are its penetration rate and binding time. Medawar was the first to demonstrate that fixatives obey diffusion laws, whereby the depth of penetration was proportional to the square root of time.[22] The importance of fixative binding time was highlighted by Fox *et al.*, who investigated the binding of formaldehyde to rat kidney tissue, in which 16 μm thin sections were used so that penetration would not be considered a factor in the kinetics of the reaction.[23] They found that the amount of methylene glycol that covalently bound to this tissue increased with time until equilibrium was reached at 24 h. Thus, binding time is the limiting factor for tissue stabilization. These aspects of chemical fixation (penetration rate and binding time) may be a

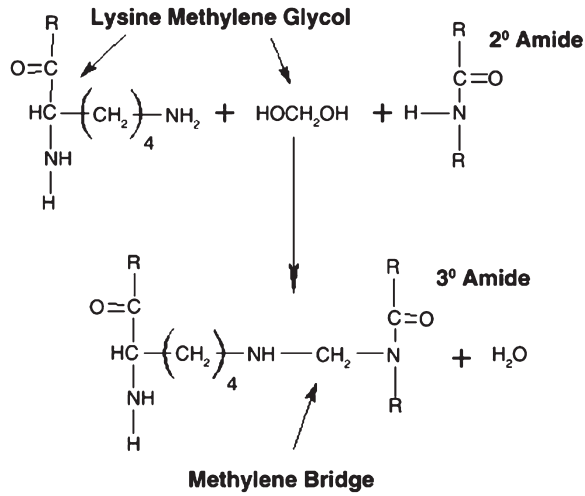

Figure 5.2 Scheme illustrating the formation of a methylene bridge during formalin fixation. (Reproduced from reference [9].)

AQ2

potential source of biomolecular variance in pathological samples, since there exists a time lag in fixative exposure and binding between cells located within the core of the tissue compared with those at the extreme dimensions of the block.[23] In fact, Fox *et al.* reported that cells at the periphery of the tissue exhibit different morphological properties from cells that are a few tenths of a millimetre further within the specimen.[23]

Compared with fresh tissue, Raman spectra of formalin fixed tissue, following 24 h fixation, exhibit a significantly reduced intensity of the Amide I peak as well as the appearance of a peak at 1490 cm^{-1}.[9] The reduced intensity of the Amide I peak is attributed to the formation of tertiary amides (and loss of secondary amide), resulting from the reaction of methylene glycol (in formalin) cross-linking the nitrogen atom of lysine with the nitrogen atom of a peptide linkage (Figure 5.2).[9] The peak at 1490 cm^{-1} is thought to arise as a result of protein unravelling and increased activity of the NH_3^+ deformation mode. However, it has also been suggested[9] that the coupling of the C–N stretching vibration with the in-phase C–H bending in amine radical cations, which may be present in the methylene bridge following formalin fixation involving lysine (see Figure 5.3, below), could result in a peak at 1490 cm^{-1}. Thus, although previous FTIR based studies of formalin fixation of isolated proteins have demonstrated no measurable effects on protein secondary structure (the arrangement of the polypeptide backbone),[24] the data above suggest that it does have an effect on protein intensity. However, contrary to previous findings on isolated proteins,[24]

AQ1

Faoláin *et al.* found that formalin fixation of tissue produced a notable shift of 10 cm^{-1} in the Amide I and II bands in FTIR spectra.[9]

Formalin fixation was also found to preserve lipid signals in Raman spectra of lipid rich tissue such as adipose tissue and white matter of the brain.[8] Both

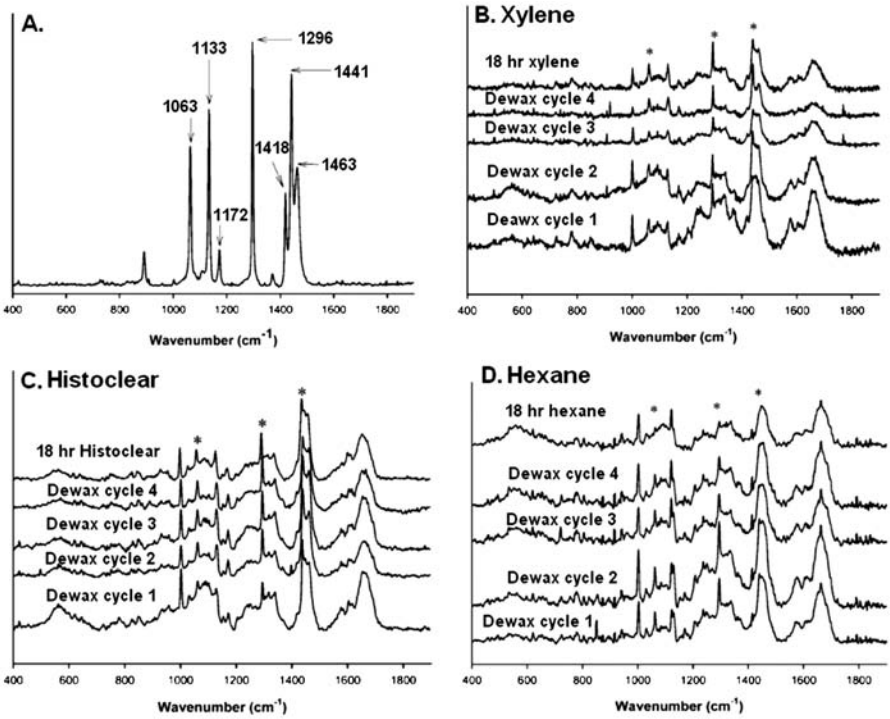

Figure 5.3 (A) Raman spectrum of paraffin wax; Raman spectra of paraffin embedded tissue following treatment with repeated cycles of deparaffinization agents (B) xylene, (C) Histoclear and (D) hexane. * Marker peaks corresponding to paraffin residue at 1063 cm^{-1}, 1296 cm^{-1} and 1441 cm^{-1}. Modified with permission and reproduced from reference [28].[28]

Huang *et al.*[10] and Shim and Wilson[8] reported that a direct spectral contaminant from formalin in the Raman spectrum is a weak peak appearing at 1040 cm^{-1}. However, this artefact can be successfully removed through copious washes with PBS.[9]

Pleshko *et al.*[11] have shown that 70% ethanol fixation of 35-day-old embryonic rat femur gave rise to FTIR spectra that exhibited Amide I and II peaks that were shifted to lower frequencies (1647 cm^{-1} and 1546 cm^{-1}, respectively) compared with unfixed rat femur, which exhibited Amide I and II peaks at 1651 cm^{-1} and 1550 cm^{-1}. It was concluded that evaluation of protein structure in this tissue should be limited to snap-frozen samples, or formalin-fixed tissues where there were no observable shifts in the Amide I and II peaks. Although this does not conform to the observations made by Faoláin *et al.*,[9] this difference may be due to the different types of tissue used in each study, calcified tissue in Pleshko *et al.*[13] and non-calcified tissue in Faoláin *et al.*[9]

AQ1

AQ1

Further studies of the effects of sample preparation on bone tissue were undertaken by Aparicio *et al.*[25] and Yeni *et al.*[26] In the study by Aparicio

et al.,[25] seven different fixatives, absolute ethanol, 70% ethanol, glycerol, formaldehyde, EM fixative, and formalin in cacodylate or phosphate-buffered saline, and six different commonly used embedding media, Araldite, Epon, JB-4, LR White, PMMA and Spurr, were assessed by FTIR microspectroscopy. The FTIR spectra were compared with those from unprocessed ground tissue and with cryosections of unfixed tissue, fast-frozen in polyvinyl alcohol (5% PVA). Non-aqueous fixatives and embedding in LR White, Spurr, Araldite and PMMA were found to have the least effect on the spectral parameters measured (mineral to matrix ratio, mineral crystallinity and collagen maturity) compared with cryosectioned and non-fixed, non-embedded tissue.

In the study by Yeni *et al.*,[26] the effects of two fixatives, ethanol and glycerol, and six embedding media, Araldite, Eponate, Technovit, glycol methacrylate, polymethyl methacrylate and LR White, on the Raman spectral properties of bone were investigated. Non-fixed, freeze-dried and fixed but not embedded tissue samples were also included. Significant effects of fixation and embedding were observed and no single combination of fixative and embedding medium that left all spectral features unaltered was found. As found for the FTIR study by Aparicio *et al.*,[25] careful selection of a fixation/embedding combination for bone tissue is recommended to allow measurement of the spectral features of interest.

5.2.4 Paraffin Embedded Tissue

As mentioned in section 5.2.1, fixed tissue is immersed in xylene prior to impregnation with paraffin wax. Faoláin *et al.* have shown that Raman spectra of formalin fixed tissue exposed to xylene produce a number of strong peaks, associated with the aromatic structure, at 620 cm^{-1} (C–C twist of aromatic rings), 1002 cm^{-1} (C–C stretching of aromatic rings), 1032 cm^{-1} (C–C skeletal stretch of aromatic rings), 601 cm^{-1} (C–C in plane bending of aromatic rings) and 1203 cm^{-1} (C–C_6H_5 stretching mode of aromatic rings).[9] As mentioned in section 5.2.3, formalin fixation was found to reduce the intensity of the Amide I band. Interestingly, upon xylene exposure, the Amide I band was observed to reappear with appreciable intensity. It was suggested that the cross-linking of proteins by methylene glycol is reversed upon xylene treatment so that the Amide I band reverts back to the secondary amide.[9] As expected, the FTIR spectrum of xylene-treated formalin-fixed tissue demonstrated a loss of the lipid ester (C=O) band at 1740 cm^{-1}, due to significant removal of cellular lipids.

Presently in the field of FTIR or Raman spectroscopy, there is lack of consensus with regard to a standard protocol for deparaffinization of paraffin embedded sections, and several approaches have been used. For example, Fernandez *et al.* deparaffinized prostate tissue sections by immersing in hexane at 40 °C with continuous stirring for 48 h.[7] During this period, the vessel was emptied every 3–4 h, rinsed thoroughly with acetone followed by hexane, and after thorough drying refilled with fresh hexane to promote dissolution of paraffin embedded in the tissue. The disappearance of a peak at 1462 cm^{-1} in the FTIR spectrum was used to ensure complete deparaffinization.

Sahu *et al*. deparaffinized samples of colon tissue using xylene and alcohol. The 10 μm paraffin embedded sections were washed with xylol for 10 min (three changes) with mild shaking.[27] Following this, the slide was washed with 70% alcohol for 12 h. To evaluate the efficacy of this procedure, FTIR spectra from the tissue were collected at each stage of the deparaffinization process: before deparaffinization, at each xylol washing step (following air-drying), and following alcohol treatment. It was reported that following two washes with xylol, a third xylol wash did not produce any significant changes to the lipid spectral regions (2800–3000 cm^{-1} and 1426–1483 cm^{-1}). Further treatment with alcohol produced changes to the region 900–1185 cm^{-1}, which was speculated to be the result of residual xylene removal. Alcohol treatment also showed a further reduction in lipid hydrocarbon signals in the spectral region 2800–3000 cm^{-1}. The authors observed that haematoxylin and eosin (H&E) sections of these deparaffinized tissues exhibited clear outlines for the cells that indicated the preservation of lipids in complex forms (membranes).

AQ1 Faoláin *et al*. deparaffinized parenchymal tissue sections by immersing in two baths of xylene for 5 and 4 min, respectively, followed by two baths of absolute ethanol for 3 and 2 min and a final bath of industrial methylated spirits 95% for 1 min.[9] This method was found through Raman microspectroscopy to be inefficient at removing all of the paraffin since a number of strong signals from C–C and CH_2 vibrational modes were observed.[9]

AQ1 Contrary to Fernandez *et al*.[7] and Sahu *et al*. [27],[27] Faoláin *et al*. suggested that complete removal of paraffin from the tissue section is not possible to assess accurately with FTIR spectroscopy using the $\sim$1462 cm^{-1} signal.[9] This was concluded following analysis of Raman and FTIR spectra obtained from deparaffinized tissue sections (using an identical deparaffinization protocol for each mode of analysis) in which spectral peaks characteristic of paraffin were clearly resolved in Raman spectra (strong sharp bands), compared with FTIR AQ1 spectra.[9] A follow-up study by Faoláin *et al*. comprehensively evaluated the efficiency of different deparaffinization agents to remove paraffin wax from cervical tissue sections.[28] In this study, one deparaffinization cycle involved two baths of deparaffinization agent (5 min and 4 min, respectively), followed by immersion in two baths of ethanol (3 min and 2 min, respectively) and a final bath in industrial methylated spirits 95%. This Raman based investigation demonstrated that paraffin signals at 1063 cm^{-1} (C–C stretch), 1296 cm^{-1} (CH_2 deformation) and 1441 cm^{-1} (CH_2 bending) (Figure 5.3A) were not completely removed by xylene and Histoclear even after 18 h of treatment (Figure 5.3B–C). However, hexane was found to be a superior deparaffinization agent, removing nearly all of the paraffin 18 hours post treatment (Figure 5.3D). These important findings were found to have practical implications for immunohistochemical staining. It was found that the intensity of positive staining in tissue sections treated with hexane for 18 h was 28% greater than in adjacent sections treated with xylene for the same period.[28] A more recent study confirmed that hexane was the most efficient dewaxing agent compared with xylene, histolene, cyclohexane, diethylether and 1.7% dishwashing soap, and showed conclusively that full deparaffinization by

hexane resulted in improved immunohistochemical staining in rat oesophagus, skin, kidney and liver tissue [29].[29]

AQ1 In the light of these findings from Faoláin *et al.*,[28] the protocol used by Fernandez *et al.*, where prostate tissue sections were treated with hexane for 48 h,[7] provides the most efficient method of paraffin removal used in an FTIR study to date. In fact, using this sample preparation protocol high levels of accuracy ($\geq 90\%$) were achieved for classifying a number of different tissue components for FTIR chemometric imaging of prostate tissue microarrays. Nevertheless, it has been shown by Gazi *et al.*,[30] who used a less rigorous method of deparaffinization involving Citroclear, which is less toxic than xylene, that the spectral region between 1481 cm^{-1} and 999 cm^{-1} could be used to discriminate and classify the different pathological grades of prostate cancer. A statistically significant distinction between tumours localized to the prostate gland and those showing extracapsular penetration could also be made. Moreover, the time efficient method of less rigorous deparaffinization is suitable for other FTIR based diagnostic parameters that do not include spectral regions that overlap with paraffin signals, such as the peak area ratio of the 1030 cm^{-1} (glycogen) to 1080 cm^{-1} (phosphate) bands, which differentiated malignant from benign prostate tissues in imaging studies.[31]

A recent study, by Meuse and Barker,[32] used FTIR spectroscopy to assess paraffin removal based on CH stretching bands near 2850, 2918 and 2956 cm^{-1}. Hexane, xylene and limonene were compared as dewaxing agents and two human breast cancer cell lines were used as model tissues. With all three dewaxing agents, at least 97% of paraffin was found to be removed, with xylene

AQ1 found to be the most effective. The difference from the study by Faoláin *et al.*[28] is more than likely due to the fact that cell cultures were used, which would not have the complex intracellular components of tissue samples.

It may be argued that, for FTIR and Raman studies, the removal of paraffin is not necessary at all as only discrete frequency ranges corresponding to the lipid hydrocarbon modes are affected.

A number of studies have shown that non-dewaxed FFPP sections can be used successfully for skin and colon tissues.[33–37] For FTIR imaging, extended multiplicative signal correction (EMSC) was used to correct the spectral contribution from paraffin and PCA was used to improve the EMSC efficiency.[36,37] For Raman spectroscopy, independent component analysis (ICA) was used to obtain model sources of paraffin, and a spectral unmixing method, the non-negativity constrained least squares (NCLS) method, was used to eliminate the paraffin contribution from each individual Raman spectrum.[33–35] Untereiner *et al.* used FTIR imaging to compare FFPP sections without any dewaxing to frozen sections of peritoneal tissues and showed that sample preparation did not affect the discriminative potential of the technique.[38]

However, visualization of the unstained tissue's anatomical features has been shown to be severely hampered if the paraffin is not removed. Sahu *et al.* reported that colonic crypts in a 10 μm paraffin embedded tissue section appeared as circular entities when viewed under light microscopy.[27] Moreover, even between adjacent microtomed sections, tissue components can vary

Table 5.1 Summary of the main FTIR and Raman bands affected by standard tissue processing protocols used for histopathology.

	Main FTIR bands affected	*Main Raman bands affected*
Drying		Decrease in intensity of the 930 cm^{-1} peak, and an increase in the lipid:protein signal[20]
Cryopreservation	Overall reduction in intensity, shifts in the Amide I and II bands[19]	Reduction in the intensity of 1002[1], 1447 and 1637 cm^{-1} bands[19]
Formalin fixation	Shift of 10 cm^{-1} in the Amide I and II bands[19]	Reduced intensity of the Amide I peak,[19] and appearance of a peak at 1490 cm^{-1}
Paraffin embedding	1465 cm^{-1} band[19] 2850, 2918 and 2956 cm^{-1} bands[32]	1063, 1130, 1296 and 1436 cm^{-1} bands[19]

significantly, which in turn prevents the positioning of the beam upon a specific tissue location by comparison with an H&E section.

In Table 5.1 a summary of the main findings from section 2 is presented. The main FTIR and Raman bands affected by tissue drying, cryopreservation, formalin fixation and paraffin embedding are listed as these are the standard tissue processing methods used for histopathology.

5.3 Cell Preparation

5.3.1 Introduction to Cell Preparation Methods

Cells are naturally present in a hydrated form, whereby water molecules are bound to macromolecules such as proteins, phospholipids and carbohydrates and this contributes to their structural integrity and function. A review of the early literature concerning the application of FTIR to cell analysis for diagnostic or imaging purposes reveals that cells had generally been prepared by direct culture upon infrared (IR) transparent substrates, followed by removal from the culture medium and air-drying.[39–44] However, the air-drying process causes delocalization of biomolecules as a result of large surface tension forces associated with passing the water–air interface. Other researchers in the field have prepared cells by removing them from culture medium and then centrifugation,[45] drying under nitrogen gas,[46] or cytospinning,[47] with the view of minimizing the effects of these surface tension forces by increasing the rate of dehydration.

The removal of cells from pH buffered growth medium and subsequent air-drying can influence the osmotic pressure within these cells, resulting in cell shrinkage or swelling with the latter resulting in membrane rupture and leaching of intercellular components. In addition, drying of living cells can

initiate autolytic processes whereby intracellular enzymes contained within lysosomes cause denaturing of proteins and dephosphorylation of mononucleotides, phospholipids and proteins. Furthermore, autolysis involves chromatin compaction, nuclear fragmentation (involving RNA and DNA nucleases) and cytoplasmic condensation and fragmentation. Thus, in FTIR based biomechanistic studies, where researchers are interested in identifying the metabolites formed as a result of the cell's response to specific stimuli, the effects of autolysis as a consequence of inappropriate cell preparation may obscure these investigations.

In cell biology, a critical and fundamental step in any investigation is "fixation". This is used to quench autolysis, minimize leaching of biomolecular constituents, whilst at the same time using optimized dehydration protocols to bypass surface tension distortions and preserve the structural and functional chemistry of biomolecules for analysis.

Another fundamental aspect of sample preparation that can influence cellular biochemistry is the surface on which they are grown. The surface can induce changes in cell adhesion and motility, in their proliferation and differentiation and in gene expression. It is desirable for *in vitro* cultures to mimic the *in vivo* environment as closely as possible and, in this context, progress has recently been made in modelling cellular systems in two-dimensional cultures. Studies have also been carried out detailing the use of biomaterial surfaces (Matrigel™, fibronectin, laminin, gelatin) for this type of cell culture. The influence of these surfaces on cell morphology and the spectral information obtained is also discussed.

5.3.2 Chemical Fixation of Cells

As mentioned in section 5.3.1, to avoid potential confounding variables from autolytic processes initiated by cells during air-drying, it is important that the cells are appropriately fixed to maintain localizations of biomolecular species. To this end, Gazi *et al.* studied the use of three chemical fixation methods for spectroscopically mapping single prostate cancer cells with synchrotron (SR) based FTIR microspectroscopy.[48] The cells were cultured directly onto MirrIR reflection substrates for transflection mode analysis. In the first method, the cells were fixed in 4% formalin (in PBS) for 20 min at room temperature with a brief rinse in doubly deionized water (3 s) before being air-dried. Water rinsing was found to be an important step for removing residual PBS from the surface of the cells so that a clear distinction could be made between the nuclear and cytoplasmic compartments (Figure 5.4A–B). This also reduced light-scattering artefacts during analysis. Although trypan blue staining of these cells demonstrated loss of plasma membrane integrity, which is likely to be due to the 1% methanol present in the fixative, SR-FTIR images (collected with 7 μm×7 μm sampling-aperture-size and 3 μm step-size) revealed localizations of lipid [ν_s(C=O)] and phosphate [$\nu_{as}(PO_2)$] domains (Figure 5.4C). Spectral subtraction of the neat formalin spectrum from the FTIR spectrum of the formalin

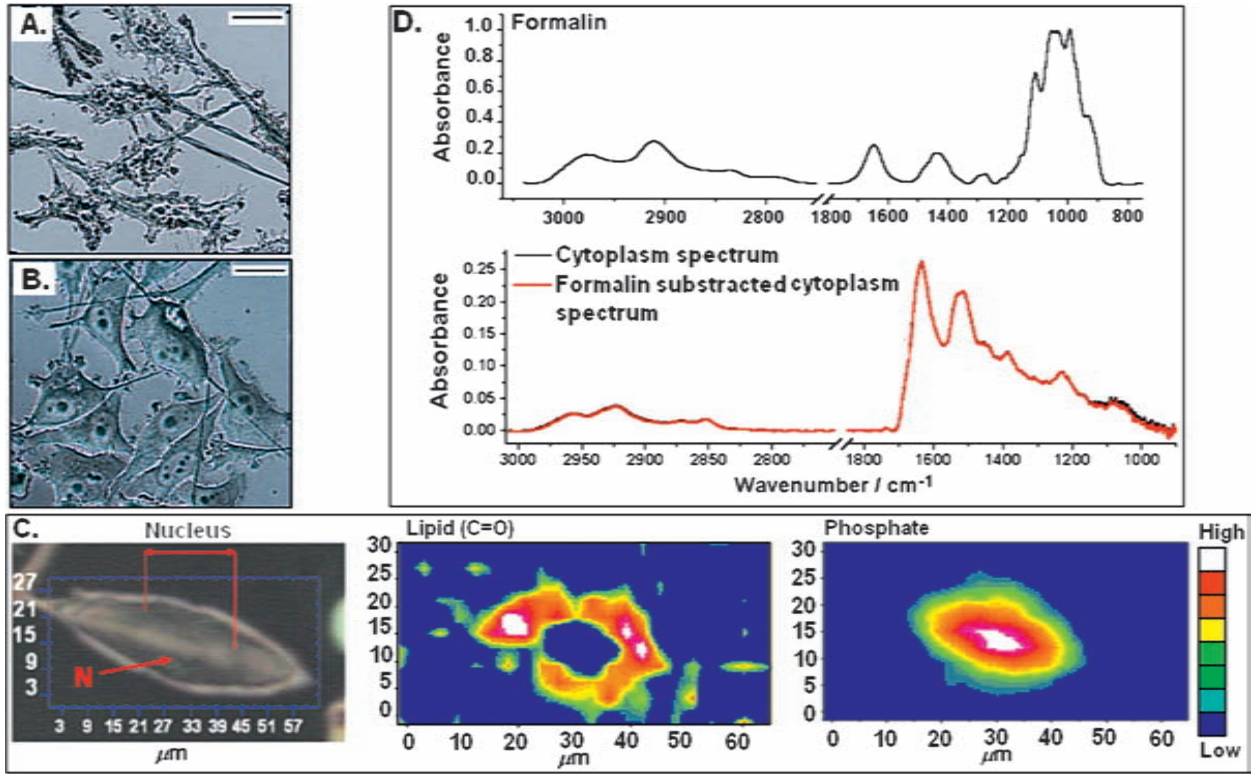

Figure 5.4 Photomicrographs of formalin-fixed prostate cancer cells, (A) without subsequent rinsing in deionized water and (B) with 3 s rinse in deionized water to remove residual PBS from the surface of the cells. Scale bar in all photomicrographs = 50 μm. (C) Optical image of a single, formalin-fixed, PC-3 cell. The cell's nucleus and nucleolus (N) are identified. SR-FTIR images depicting the intensity profiles of lipid ester v_s(C=O) (1752–1722 cm^{-1} peak area) and phosphate $v_{as}(PO_2)$ (1280–1174 cm^{-1} peak area). (D) The FTIR spectrum of formalin and overlay of the FTIR spectrum of the cytoplasm with the same spectrum processed to remove their theoretical formalin content. (Reproduced from reference [48].)

AQ2

fixed cell resulted in negligible differences in the intensities of peaks across the frequency range 3000–1100 cm^{-1} (Figure 5.4D). This was performed following normalization of the spectrum of formalin to the intensity value of the peak at 1000 cm^{-1} in the formalin fixed cell spectrum, since this frequency gives rise to the most intense peak in the spectrum of formalin.

In the second method, cells were formalin fixed and subsequently critical point dried (CPD). The CPD process involves first displacing gradually the intercellular water molecules in the formalin-fixed cells with increasing concentrations of ethanol. The ethanol is then displaced by acetone, which is miscible with liquid CO_2. The acetone within the cells is then displaced by liquid CO_2, within a chamber. The chamber is heated with a simultaneous rise in pressure as liquid CO_2 enters the vapor phase. At a specific temperature and pressure, the density of the vapor equals the density of the liquid, the liquid–vapor boundary disappears, and the surface tension is zero. Thus, this method reduces any residual distortions that may occur in the pre-fixed cell as a result of air-drying. Since the formalin fixed CPD dried cells were exposed to significant lipid-leaching reagents (ethanol and acetone), the cells were positive to trypan blue staining and the SR-FTIR spectrum of these cells demonstrated loss of the lipid ester ν_s(C=O) peak.

In the third fixation method cells were fixed with glutaraldehyde and osmium tetroxide (OsO_4) prior to CPD. Glutaraldehyde polymerizes in solution, where dimers and trimers are the most abundant polymers.[49] The aldehyde groups of glutaraldehyde react with the amino groups of proteins to form imines in an irreversible reaction. The commonly used post-fixative to glutaraldehyde is OsO_4, which preserves unsaturated lipids by the formation of cyclic esters and is also an irreversible reaction.[49] With the exception of a weak peak at 960 cm^{-1}, it also does not give rise to absorption bands within the spectral region of interest in the mid-IR range where most biomolecules absorb. CPD–glutaraldehyde–OsO_4 fixation of cells preserves fine structure as observed in electron microscopy studies. The cells were found to be negative to trypan blue, indicating good preservation of plasma membrane lipid molecules. Various SR-FTIR images of cells fixed using this method (optical image in Figure 5.5A) are shown in Figures 5B–C. The neat FTIR spectrum of glutaraldehyde is shown in Figure 5D and a spectrum obtained from the SR-FTIR image of the cell is also presented. The localizations of phosphate and lipid ester ν_s(C=O) signals were consistent with SR-FTIR maps of formalin fixed cells (see Figure 5.4). Although no significant spectral markers from glutaraldehyde were detected in the SR-FTIR spectrum of these cells, compared with formalin fixed cells (see Figure 5.4D), a reduction in the intensity of peaks between 1500 cm^{-1} and 1000 cm^{-1} was observed and the lipid ester ν_s(C=O) signal appeared as a less resolved shoulder on the amide I band (Figure 5.5D).

Harvey *et al.* compared formalin fixation and alcohol fixation (SurePath preservative for liquid based cytology) for prostate cells in culture.[50] Formalin fixed cells showed a better diagnostic performance. This was, however, primarily due to the Raman tweezers experimental set-up. A much lower laser power was used for SurePath fixed cells because of problems with cells escaping

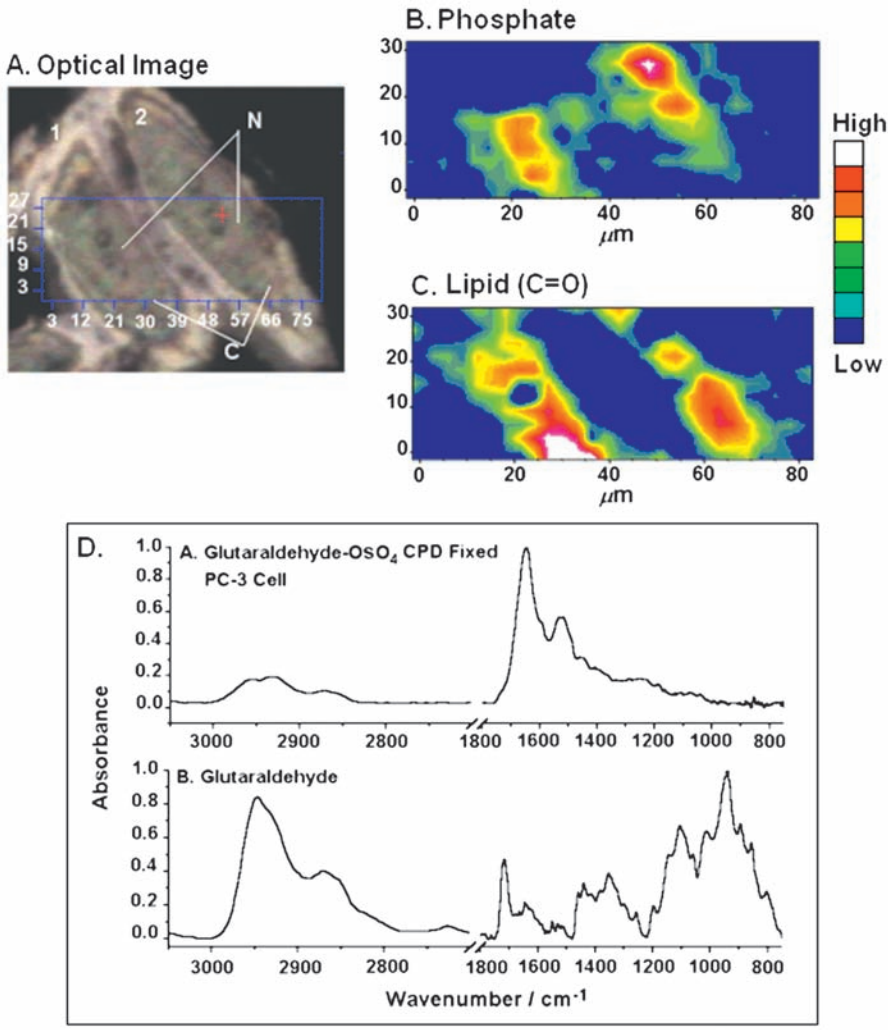

Figure 5.5 (A) Optical image of two glutaraldeyde–osmium tetroxide critical point dried (CPD) fixed PC-3 cells (labelled 1 and 2). N designates the nucleus, C designates the cell cytoplasm. Localizations and intensity profiles of (B) phosphate (1271–1180 cm^{-1} peak area) and (C) lipid ester (C=O) (1756–1722 cm^{-1} peak area). (D) FTIR spectrum of a glutaraldehyde–osmium tetroxide fixed PC-3 cell; the IR spectrum of neat glutaraldehyde. (Reproduced from reference [48].)

AQ2

the laser trap. This resulted in much lower signal to noise ratios for SurePath fixed cells, leading to better prediction rates for formalin fixed cells.

Mariani *et al.* compared the effects of light fixation in 2% formalin, air drying and desiccation for 1 h each on two different cell lines using Raman spectroscopy.[51] For human keratinocyte cells (HaCaT cell line), air dried

samples provided the best intensity for all components. Desiccation produced a slightly less intense spectral profile when compared with air-drying. Both air-drying and desiccation maintained significant spectral features particularly in the 1600–1500 cm^{-1} region. Formalin fixation produced the weakest overall spectrum with many of the less intense features becoming largely unidentifiable, particularly in the 1600–1500 cm^{-1} region. However, formalin fixation was found to be the most consistent method of cell preservation, with air-drying found to be the most inconsistent method. For activated human peripheral macrophages, C.A.MM6 cells, the most intense spectra were from formalin fixed and desiccated samples. Lower intensity bands detected in the spectra of desiccated and formalin fixed samples from 1253 cm^{-1} to 1127 cm^{-1} specific for mostly lipid and protein constituents could not be identified in the air-dried sample. Despite the preservation of many important strong and weaker spectral features in the C.A.MM6 cells with formalin fixation, overall reproducibility of this fixation method was found to produce significant inconsistencies. These inconsistencies resulted from the differential distribution of cell surface proteins and lipid conformations present. This was found to be particularly important for C.A.MM6 cells because activated cells express more proteins and undergo significant plasma membrane changes compared with non-activated cells. Structural component organization and lipid conformations are also known not to be identical between individual cells of the same lineages. These inter-lineage differences can vary in response to fixation, leading to varied methylene protein cross-linking. Air-drying and desiccation were found to be more consistent methods of cell preservation for these cells. In general, desiccation was found to provide the best compromise between signal intensity and preservation of cellular components.

A more recent study made the important step of using live cells as a reference for evaluation of fixation effects.[52] This study compared the effects of three commonly used fixatives, formalin, Carnoy's fixative (60% absolute ethanol, 30% chloroform, 10% glacial acetic acid) and methanol:acetic acid (3:1), on three cell lines using Raman spectroscopy. The level of fixation effect was found to be cell line dependent but, in general, all the fixatives were observed to affect the vibrational modes of lipid, protein, nucleic acid and carbohydrate moieties. On examination of the difference spectra and the spectral loadings and the results of k-means cluster analysis, it was concluded that formalin fixation produces a cellular spectrum that is globally more similar to that of the live cell, and therefore best preserves cellular integrity, out of the fixatives studied. Interestingly, Carnoy's fixative and methanol:acetic acid were found to affect nucleic acid spectral contributions significantly, despite being recommended for preservation of nucleic acids (Figure 5.6).

Chemical fixation was investigated for the preparation of adipocytes for FTIR analysis.[53] Adipocytes are specialized for the synthesis and storage of fatty acids (FAs) as triacylglycerides (TAGs) as well as for FA mobilization through lipolysis. Figure 5.7A shows the appearance of adipocytes in growth medium and illustrates the presence of numerous lipid droplets contained within their cytoplasm. Figure 5.7B shows adipocytes, prepared for FTIR

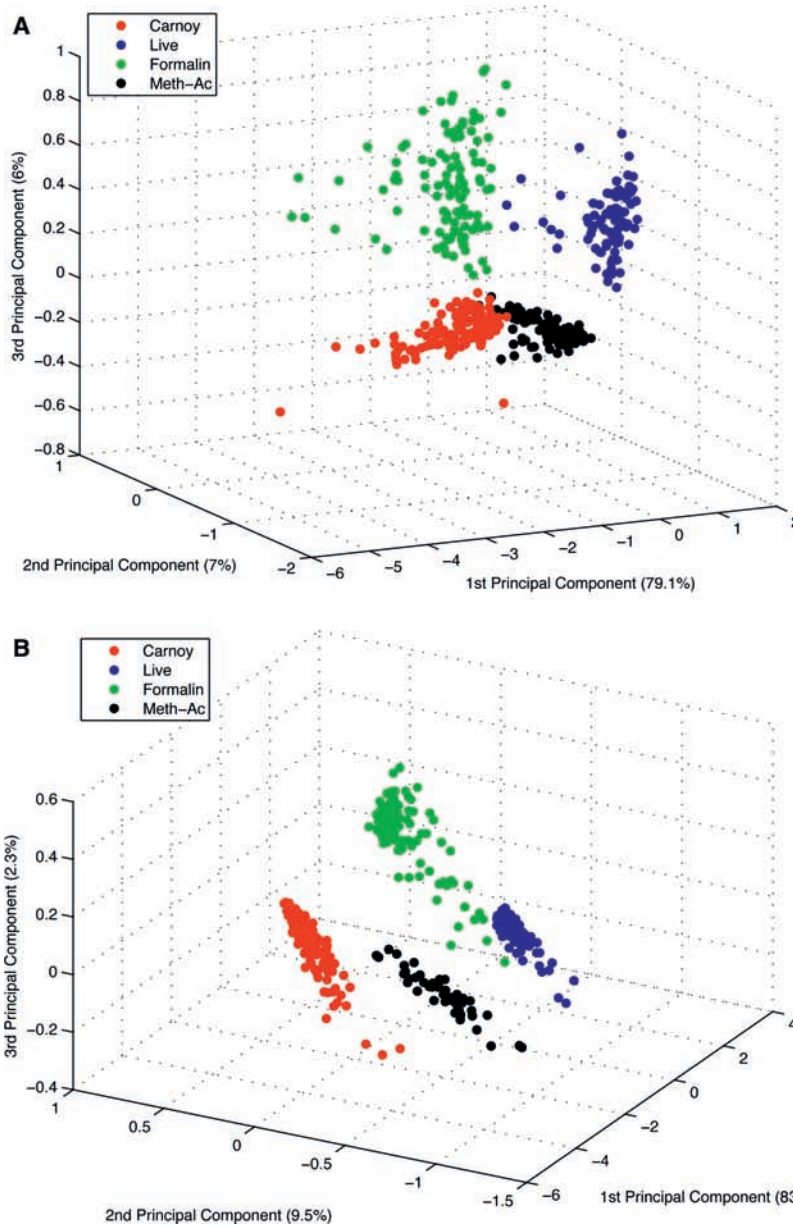

Figure 5.6 Principal components analysis (PCA) score plot for Raman spectra of (A) A549, (B) BEAS2B and (C) HaCaT cell lines. Percentage labels on each axis denote the variance described by that PC. There is clear separation of cellular spectra fixed with Meth-Ac and Carnoy's fixative relative to live and formalin fixed spectra. A degree of similarity between the spectral content of formalin fixed and live cell spectra is implied by the proximity of their clusters. (Reproduced from reference [52].)

AQ2

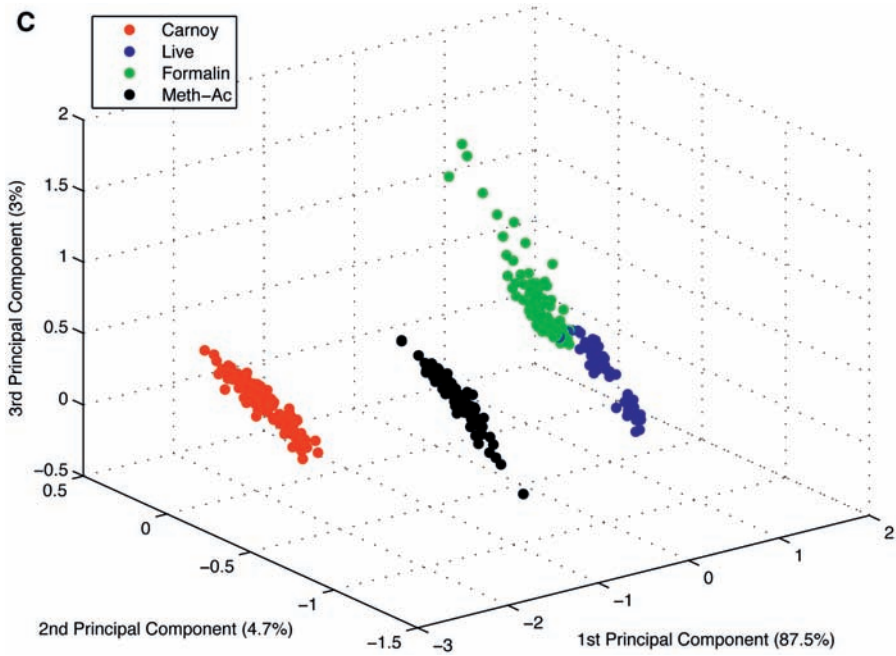

Figure 5.6 Continued.

analysis, following fixation in 4% formalin (in PBS), a brief water rinse to remove residue salts and air-drying at ambient conditions. Although this fixation protocol was appropriate for the preservation of prostate cancer cells for SR-FTIR analysis, it resulted in the collapse of intracellular lipid droplet structures into an unordered lipid deposit in the adipocytes (Figure 5.7B).

An FTIR spectrum of the intracellular lipid droplet of the formalin fixed air-dried adipocyte [Figure 5.7D(ii)] exhibits a lipid ester ν_s(C=O) peak at 1744 cm^{-1}, which is the same frequency of absorption as the lipid ester ν_s(C=O) peak in the reference TAG spectrum [Figure 5.7D(i)]. Several other characteristic peaks of the glycerol moiety of TAG are also observed in the lipid deposit of the formalin-fixed adipocyte at frequencies $>1500\,cm^{-1}$ and these are identified in Figure 5.7D(ii) as peaks labelled 8–12. However, the peaks in this spectrum [Figure 5.7D(ii)] are broader than the same peaks in the reference TAG spectrum [Figure 5.7D(i)]. This is due to collapse of the lipid droplets that give rise to a range of bonding strengths with neighbouring molecular species for those functional groups absorbing at frequencies $>1500\,cm^{-1}$. Figure 5.7C shows adipocytes containing well-preserved lipid droplets following paraformaldehyde (PF) fixation with OsO_4 post-fixation and CPD.

The advantages of this sample preparation over formalin fixation, water rinsing and air-drying are: (a) formalin in PBS contains methanol, which permeates the plasma membrane and results in a faster fixation compared with PF that does not contain methanol. However, methanol extracts intracellular

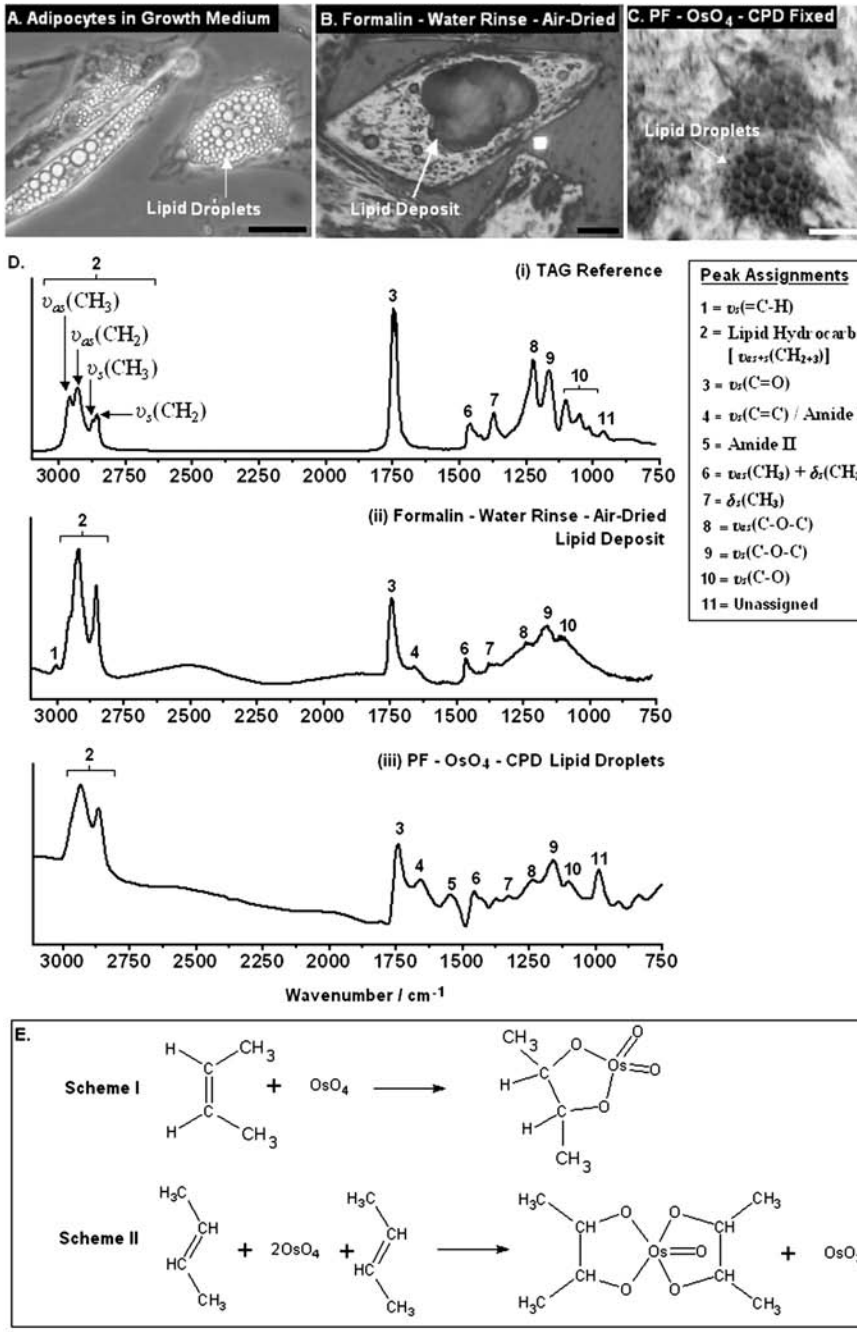
A. Adipocytes in Growth Medium
Lipid Droplets
B. Formalin - Water Rinse - Air-Dried
Lipid Deposit
C. PF - OsO4 - CPD Fixed
Lipid Droplets
D.
(i) TAG Reference
(ii) Formalin - Water Rinse - Air-Dried Lipid Deposit
(iii) PF - OsO4 - CPD Lipid Droplets
Wavenumber / cm-1
Peak Assignments
1 = υs(=C-H)
2 = Lipid Hydrocarbon [υas+s(CH2+3)]
3 = υs(C=O)
4 = υs(C=C) / Amide I
5 = Amide II
6 = υas(CH3) + δs(CH2)
7 = δs(CH3)
8 = υas(C-O-C)
9 = υs(C-O-C)
10 = υs(C-O)
11 = Unassigned
E.
Scheme I
Scheme II

lipids, which is inappropriate for adipocyte fixation. (b) The OsO_4 post-fixative preserves lipids. (c) The 3-dimensional structure of the adipocyte is retained since the sample is dried without surface-tension effects, through CPD, and the localization of intracellular lipid droplets of the adipocyte is persevered. The disadvantage of this fixation protocol is that the mode of action by which OsO_4 preserves lipids is through complexation reactions within the double bonds of lipid hydrocarbon chains or complexation and cross-linking between unsaturated hydrocarbon chains (Figure 5.7E). Thus, the $\upsilon_s(=C–H)$ signal from unsaturated hydrocarbons is present in the lipid-deposit spectrum of the formalin fixed, water rinsed, air-dried adipocyte [Figure 5.7D(ii)], but is not observed in the lipid-droplet spectrum of the PF–OsO_4–CPD adipocyte [Figure 5.7D(iii)]. Additionally, both methods of fixation (formalin–water rinse–air-dried and PF–OsO_4–CPD) result in a decrease in peak resolution of the $\upsilon_{as}(CH)_2$ and $\upsilon_{as}(CH)_3$ modes and the $\upsilon_s(CH)_2$ and $\upsilon_s(CH)_3$ modes.

The PF–OsO_4–CPD protocol outlined above was used to preserve samples of prostate cancer cells (PC-3 cell line; prostate cancer cells derived from bone metastases) that were co-cultured with adipocytes pre-loaded with deuterated palmitic acid ($D\text{-}PA_{31}$).[53] This specimen was used in an FTIR tracing experiment to determine whether PC-3 cells could uptake the fatty acids stored within adipocytes. Figure 5.8A shows an optical image of a PF–OsO_4–CPD fixed adipocyte surrounded by PC-3 cells and stroma cells. In this figure the adipocytes are visualized as large dark bodies (designated by Adp in Figure 5.8A), whereas PC-3 cells (1–4) are lighter in appearance and possess lamellipodia/pointed processes. The dark stain results from the binding of OsO_4 to the lipids. The boxed area was mapped using FTIR microspectroscopy, and the $\upsilon_{as}(C\text{-}D)_{2+3}$ signal intensity distribution is shown in Figure 5.5B, above. As expected, there was localization of the $\upsilon_{as}(C\text{-}D)_{2+3}$ signal with high intensity to the adipocyte; however it was also found that this signal illuminated the PC-3 cells (Figure 5.8B). Given that the only source of $\upsilon_{as}(C\text{-}D)_{2+3}$ signal in the PC-3 cells is through incorporation of D_{31}-PA released by the adipocytes, these data unequivocally demonstrate the translocation of D_{31}-PA between these cell types without cell isolation or external labelling. Appropriate fixation was necessary in this experiment, since delocalization/bleeding of lipid molecules

Figure 5.7 Optical photomicrographs showing (A) adipocytes in growth medium with prominent intracellular droplets (scale bar = 10 μm); (B) adipocyte following formalin fixation, water rinsing and air-drying (scale bar = 20 μm); (C) adipocytes fixed in paraformaldehyde (PF) and osmium tetroxide (OsO_4) and critical point dried (CPD) (scale bar = 30 μm); (D) typical FTIR spectrum of (i) triacylglyceride (TAG) reference with C_2–C_{10} saturated hydrocarbon chains, (ii) the lipid deposit from a formalin fixed air-dried adipocyte, and (iii) the lipid droplets from a paraformaldehyde (PF) and osmium tetroxide (OsO_4) CPD adipocyte; (E) OsO_4 reaction with unsaturated hydrocarbon chains to form cyclic esters. **Scheme I**. Reaction with a single unsaturated hydrocarbon chain. **Scheme II**. Cross-linking reaction with adjacent unsaturated hydrocarbon chains. (Reproduced from reference [53].)

AQ2

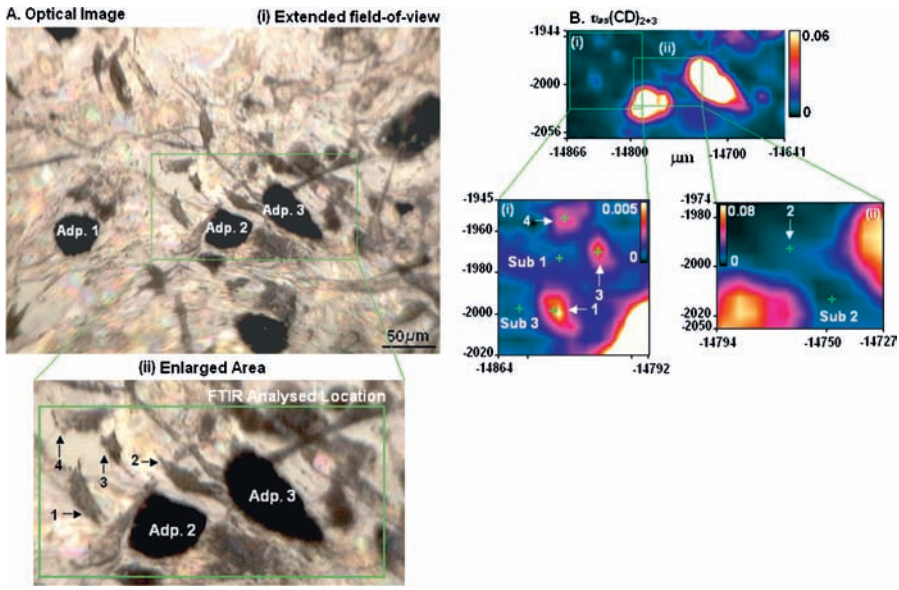

Figure 5.8 (Ai) Optical photomicrograph showing PF–OsO_4–CPD fixed adipocytes (Adp. 1–3) surrounded by prostate cancer cells and stroma cells. **(Aii)** Magnified region of Adp. 2 and 3 with surrounding prostate cancer cells (Labelled 1–4). The boxed area was analysed by imaging FTIR micro-spectroscopy. (B) FTIR spectral maps depicting the intensity distribution of the $\upsilon_{as}(C\text{-}D)_{2+3}$ signal. The boxed areas (i) and (ii) were expanded and the colour intensity threshold changed to provide better contrast of the $\upsilon_{as}(C\text{-}D)_{2+3}$ signal in cells relative to the substrate. (Reproduced from reference [53].)

from adipocytes in the adipocyte–PC-3 cell co-culture system could result in false-positive results concerning PC-3 uptake of adipocyte-derived D_{31}-PA.

A summary of the main findings from section 5.3.2 is presented in Table 5.2. The main FTIR and Raman bands affected by the commonly used cell preservation methods of drying and fixation are listed.

5.3.3 Cell Preparation for Biomechanistic Studies

In the FTIR study by Tobin *et al.*,[45] drying cells by centrifugation was used to investigate the response of cervical cancer cells to epidermal growth factor (EGF). Cells were incubated with EGF with increasing incubation times. Changes in protein conformation (noted by shifts in Amide I peak position) as a result of phosphorylation by EGF (monitored by the peak area of the phosphate monoester vibration at 970 cm^{-1}), at consecutive time points, were observed. Such a time-course experiment required a rapid method of sample preparation because of the short interval between sampling time points. Gazi *et al.* used formalin fixation to study the temporal fluctuations in phosphate,

Table 5.2 Summary of the main FTIR and Raman bands affected by standard cell processing protocols.

		Main FTIR bands affected	*Main Raman bands affected*
Drying	Air drying Desiccation		Loss of features in 1253–1127 cm^{-1} region[51] Less intense bands at 1612 cm^{-1} and 1180 cm^{-1} compared with formalin fixation[51]
Chemical fixation	Formalin	No significant effects[38], [38, Hastings *et al*. 2008]	Formalin fixation closest to live cell[52] but AQ3 line dependent[51] Nucleic acid bands (804–831, 1167, 1102–1200, 1300 cm^{-1}); protein bands (1669, 1450, 1345–1256, 1102–1200 cm^{-1}) and lipid bands (1170, 1284–1220, 1339–1305 cm^{-1})[52] Loss of features in 1600–1500 and 1448–1127 cm^{-1} regions[51]
	Formalin and critical point drying	Loss of lipid ester peak (1756–1722 cm^{-1}) due to exposure to acetone and ethanol[38]	
	Glutaraldehyde–osmium tetroxide and critical point drying	Reduction in intensity of –1000 cm^{-1} and less resolved lipid ester signal (1756–1722 cm^{-1})	AQ4
	Carnoy's fixative (60% absolute ethanol, 30% chloroform, 10% glacial acetic acid)		Nucleic acid bands (670–788, 788–840, 870, 895–898, 928, 1060–1095 cm^{-1}; protein bands (1668–1661, 1450, 1339–1305, 1247–1305, 1176 cm^{-1}) and lipid bands (1045, 1065–1062, 1070, 1176, 1300, 1339–1247, 1453–1447 cm^{-1})[52]
	Methanol:acetic acid (3:1)		Similar to Carnoy's fixative[52]
	Acetone	Loss of bands associated with cellular lipids (1740, 2925, 2854 cm^{-1}) and modifications to Amide I and II bands [Hastings *et al* 2008]	AQ3

protein secondary structures and endogenous non-isotopically labelled lipid signals following stimulation with different concentrations of D_{31}-PA and deuterated arachidonic acid (D_8-AA).[54] It was found that the shortest practical time interval between sampling points during which the cells could be fixed was 15 min. As an example, Figure 5.9A shows these biochemical fluctuations for

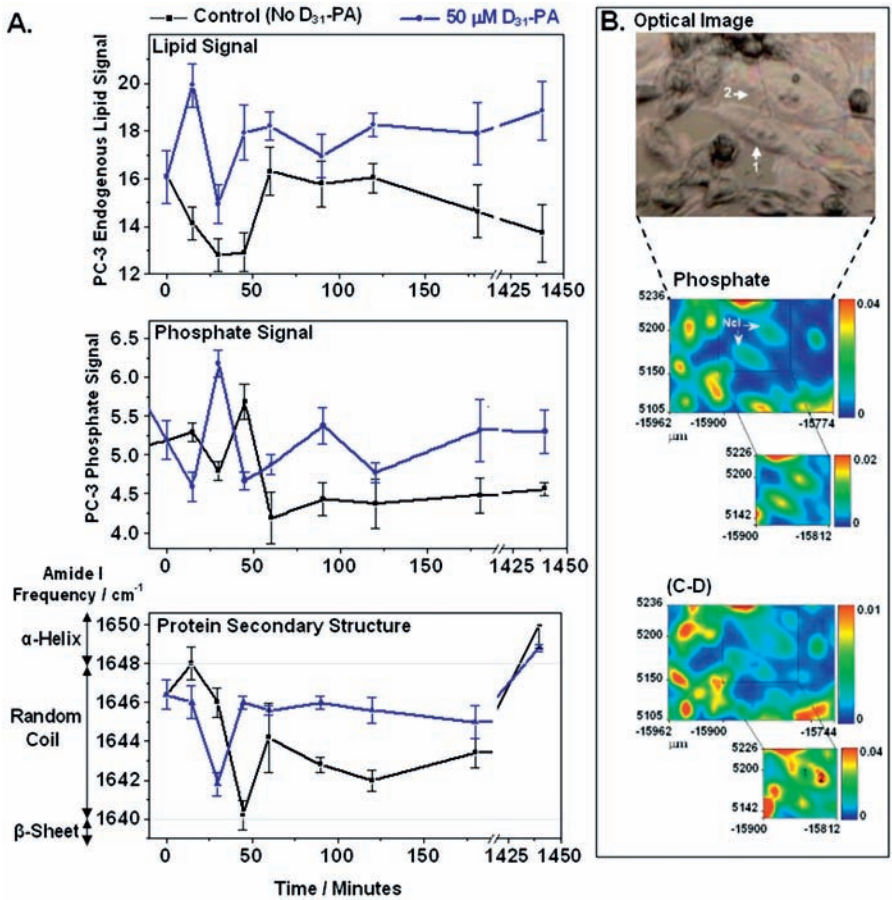

Figure 5.9 (A) Temporal fluctuations in various biomolecular domains probed by FTIR, for PC-3 cells exposed to 50 μM D_{31}-PA or no D_{31}-PA (control). Endogenous mean lipid hydrocarbon peak area intensities (±SE); mean phosphate diester peak area [$\upsilon_{as}(PO_2)$] intensities (±SE) and Amide I frequency shifts (±SE). (B) Optical image of PC-3 cells following incubation with D_{31}-PA for 24 h. This area was analysed using imaging FTIR microspectroscopy. Infrared biospectral maps show the intensity distributions of phosphate [nuclei are labelled (Ncl)] and $\upsilon_{as+s}(CD_{2+3})$ peak area (D_{31}-PA or its metabolites). In each image, cells 1 and 2 (see optical image) are magnified to demonstrate the intensity of IR signals in greater detail. FTIR spectra were obtained from points 1 (nucleus) and 2 (cytoplasm) in this image. (Reproduced from reference [54].)

AQ2

PC-3 cells incubated with 50 μm D_{31}-PA in serum-free culture media, compared with control (PC-3 cells incubated in identical conditions but without D_{31}-PA). The endogenous lipid signal in the control PC-3 cells initially fell and is induced by metabolic/cytokine/growth factor imbalance resulting from the exchange of media to serum-free RPMI media at the zero minute time-point. Conversely, cells incubated with D_{31}-PA showed an initial rise in endogenous lipids. Since the incubation medium (RPMI) contains no FAs, this increase in lipid content must be due to *de novo* biosynthesis. This initial rise in endogenous lipid signal was followed by a fall, attributed to metabolic breakdown into adenosine triphosphate (ATP), which is a major product of lipid metabolism. This notion is supported by a phosphate spike at 30 min accompanied by a significant shift in the Amide I frequency, indicating protein phosphorylation.

The time-efficient formalin fixation method not only suitably preserved biomolecular composition so that lipid metabolism and protein phosphorylation could be measured, but also preserved the subcellular localizations of biomolecules for imaging studies. Figure 5.9B shows an optical photomicrograph of PC-3 cells on MirrIR substrate, following exposure to 50 μM D_{31}-PA for 24 h. This area was analysed by imaging FTIR microspectroscopy and the resulting distribution of the integrated intensity of the phosphate diester [$\upsilon_{as}(PO_2)$; 1274–1181 cm^{-1}] peak area is shown. As expected, for cells 1 and 2 in the optical image, it can be seen that the most intense phosphate signals localize at the nucleus. In contrast, the most intense $\upsilon_{as+s}(CD_{2+3})$ signal localized at the cytoplasm, suggesting that the subcellular localization of D_{31}-PA or its metabolites is predominately in the cytoplasm.

Another FTIR based dose–response study has been undertaken where prior to spectroscopic examination, drug induced cells had been removed from culture media, washed in PBS and air-dried.[55] This study reports spectroscopic changes (ratios of peaks) that could be associated with exposure of the cells to increasing doses of the chemotherapeutic drug. Spectroscopic changes were correlated with cell sensitivity to the drug measured using the MTT [(3-(4,5-dimethylthiazol-2-yl)-2,5-diphenyltetrazolium bromide] assay. Thus, there is evidence to suggest that spectroscopic changes associated with drug exposure can be determined and that this is in fact dominant over metabolite perturbations resulting from autolysis during the drying process.

5.3.4 Growth Medium and Substrate Effects on Spectroscopic Examination of Cells

A number of studies have investigated the use of FTIR or Raman microspectroscopy as diagnostic tools to differentiate and classify cell lines, *in vitro*, based on their pathological state[56,57] or resistance to drugs.[58] Interestingly, we find that some researchers have grown their different cell lines in the same culture media,[56–58] whereas others have used different media for each cell type.[59,60] The European Collection of Cell Cultures (ECACC) provides standard protocols for the optimum growth of different cell lines. In some instances,

cell culture media may be different for cells of the same epithelial origin, for example ECACC suggest that PC-3 cells (a prostate cancer epithelial cell line derived from bone metastases) should be grown in Ham's F-12, whereas LNCaP (a prostate cancer epithelial cell line derived from lymph node metastases) should be grown in RPMI 1640. Both RPMI 1640 and Ham's F-12 are complex mixtures consisting of a range of inorganic salts, amino acids, vitamins, nucleotides and glucose as well as small-molecule precursors. However, differences among media can exist with respect to the relative concentrations of each component as well as compositional differences such as the presence or absence of a major biomolecular class, for instance RPMI 1640 contains no fatty acids, unlike Ham's F-12, which contains the ω6-FA, linoleic acid (LA).

In a recent study by Harvey *et al.*,[60] reflection mode FTIR photoacoustic spectroscopy (PAS) was used to obtain spectra from four different formalin fixed prostate cell lines (BPH = benign prostatic hyperplasia; LNCap-FGC = prostate cancer epithelial cells derived from lymph node metastases; PC-3 = prostate cancer epithelial cells derived from bone metastases; PNT2-C2 = normal prostate epithelial cells immortalized by transfection with the genome of the SV40 virus). Unsupervised principal component analysis (PCA) of this spectral data set yielded separation of clusters corresponding to each of these cell lines (Figure 5.10A). Two of these cell lines were grown in the same media (LNCaP and PNT2-C2), whereas two were grown in different media (BPH and PC-3). Importantly, the two cell lines that were grown in identical media (LNCaP and PNT2-C2) showed significant separation, realized by anticorrelation on PC-2.

In a follow-up study, Harvey *et al.* acquired conventional FTIR spectra from PC-3 cells and LNCaP cells, each grown separately in their optimum culture medium (as advised by ECACC protocols) and a "foreign medium".[61]

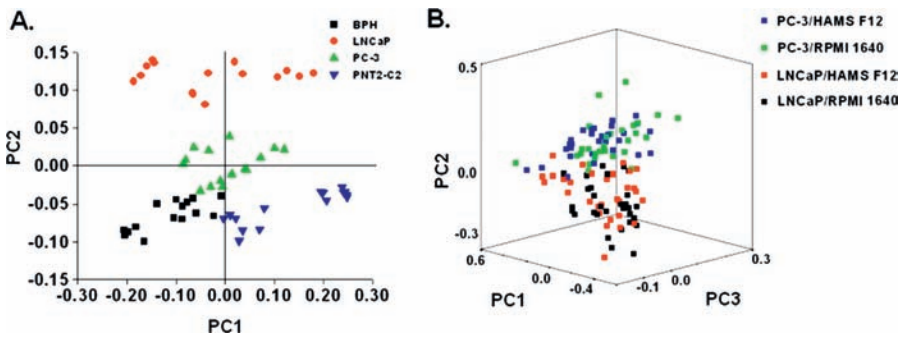

Figure 5.10 (A) Principal components analysis (PCA) scores plot of the background-subtracted, vector normalized first derivative FTIR-PAS spectra of four different prostate cell lines (BPH, LNCaP, PC-3 and PNT2-C2). (Reproduced from reference [60].) (B) PCA scores plot of vector normalized, first derivative FTIR spectra of PC-3 and LNCaP cell lines, grown in their "optimum" culture medium or "foreign" culture medium.

AQ2

Unsupervised PCA of these spectra demonstrated clustering of the two cell lines that was independent of the culture medium in which they were grown, but was principally dependent on the cell type (Figure 5.10B). Thus, it may be concluded that at least for the prostate cell lines PC-3 and LNCaP, the influence of the basic media under investigation in this study (RPMI 1640 and Ham's F-12) on the cell metabolites is not the primary influence on spectroscopic measurements. However, it must be acknowledged that cells are a function of their environment. Thus, the same cell line grown in two different media with relatively larger compositional differences (or containing potent stimuli) will affect spectroscopic classification.

If the cell is exposed to an environment that does not sustain its optimum growth and down-regulates the expression of biomolecular features (such as cell surface antigens, hormone receptors, protein expression), which characterize that cell type *in vivo*, then this may ultimately convert the cell to a new class. *In vivo*, it is well known that stromal–cell interactions are particularly important in cancers such as of the breast, where the stromal compartment plays a critical role in directing proliferation and functional changes in the epithelium.[62] Moreover, environmental stimuli directing cell phenotype have been recently studied with imaging FTIR by Krafft *et al*.[63] In this study, human mesenchymal stem cells were treated with osteogenic stimulatory factors that induced their differentiation. Differentiation was detected by FTIR through changes in the Amide I band shape (indicative of protein composition/structural changes) and phosphate levels (indicative of the expression of calcium phosphate salts).

In a similar manner to compositional differences in the growth media that may or may not elicit changes in cell biochemistry and thus its spectra, substrates can also induce morphological as well as functional changes in the cell. Meade *et al*. studied the influence of a range of substrates on the normal human epithelial keratinocyte cell line (HaCaT) using FTIR and Raman spectroscopy.[64] The substrate extracellular matrix (ECM) coatings under evaluation were two glycoproteins, fibronectin and laminin, and one protein, gelatin (derived from thermal denaturing of collagen). Gelatin was coated onto MirrIR slides for FTIR experiments or quartz slides for Raman experiments, by incubation for 24 h at 4 °C. Laminin and fibronectin were coated onto these substrates by incubation for 4 h and 40 min, respectively, at room temperature. For the fibronectin and laminin coated slides, excess solution was aspirated from the substrates and washed in PBS prior to cell deposition. For the gelatin coated slides, excess solution was aspirated and cells were deposited for culture without prior washing in PBS.

Fluorescence assays were conducted at three days post-seeding, as well as fixation using 4% formalin (in PBS) with water rinse for FTIR and Raman investigations. Cellular proliferation, viability and protein content were found to be down-regulated when cells were grown on uncoated quartz compared with uncoated MirrIR substrates. However, increases in proliferation and viability were more pronounced when cells were grown on coated quartz than coated MirrIR substrates. Additionally, it was found that quartz coated with

all three ECM coatings generated significantly enhanced proliferation compared to the control (uncoated quartz). However, this was not the case for MirrIR, which resulted in a significant increase in proliferation only for the laminin coated slide. Viability was significantly increased when cells were grown on laminin and gelatin coated quartz, whereas for MirrIR substrate, viability was only significantly increased when this was coated with gelatin. The authors suggested that gelatin provides a coating with similar proliferation effects on quartz and MirrIR and increases viability, which is desirable for long-term cultures.

The FTIR and Raman spectroscopic analyses of the coated slides demonstrated that the gelatin coating did not give rise to sufficiently high signals to significantly influence FTIR or Raman spectra of the cells cultured upon them.[64] First derivative FTIR spectra and Raman spectra of cells on gelatin, fibronectin and laminin demonstrated spectral changes on each of these substrates that were associated with nucleic acid, lipid and protein expression. Raman spectra provided further insight and relative quantification, since it was found that coatings that promoted proliferation gave rise to increases in spectral regions associated with DNA, RNA and proteins, with a decrease in lipids. This has been attributed to an increase in the sustained production of signalling proteins, as a result of integrin binding to the coating, that promotes cellular proliferation. Supporting this, the authors also found through FTIR that the ratio of protein (sum of integral absorbencies corresponding to the Amide I, II and III bands) to lipid (integral absorbance 1370–1400 cm^{-1}) gave rise to values that could be significantly correlated with an increase in proliferation (as measured by fluorescence assay).

The experimental set-up described above consisted of thin layers of ECM that were barely detectable in the FTIR or Raman spectrum; however Lee *et al.* studied prostate cancer cells that had been cultured onto relatively thicker layers of ECM.[65] In their investigation, Matrigel was used as the artificial ECM. The major constituents of Matrigel are collagen type IV (a protein), heparin sulfate (a proteoglycan), laminin and entactin (glycoproteins). Figure 5.11A shows an optical photomicrograph of prostate cancer cells on Matrigel. This area was analysed using imaging FTIR microspectroscopy. As expected, the lipid hydrocarbon signal demonstrates high intensity at the cell locations, relative to the Matrigel surroundings, due to the cumulative absorption of lipid containing biomolecules in the cells and Matrigel (Figure 5.11B). Since the lipid background signal is nearly homogeneous, it suggests that the Matrigel is of constant thickness within the analysis field-of-view. However, the protein background exhibits a heterogeneous distribution of intensity (Figure 5.11C), which is likely to be due to concentration differences when taking into consideration the lipid intensity image. As expected, cells adhered to the low protein concentration exhibited a higher protein intensity signal than the surrounding layer, whereas those on a high protein concentration or thick surface revealed an unexpected lower protein intensity signal. This is illustrated in the protein cross-section in Figure 5.11D, which was plotted with values taken from a region of high protein intensity to a region of low protein intensity and bisecting the cells.

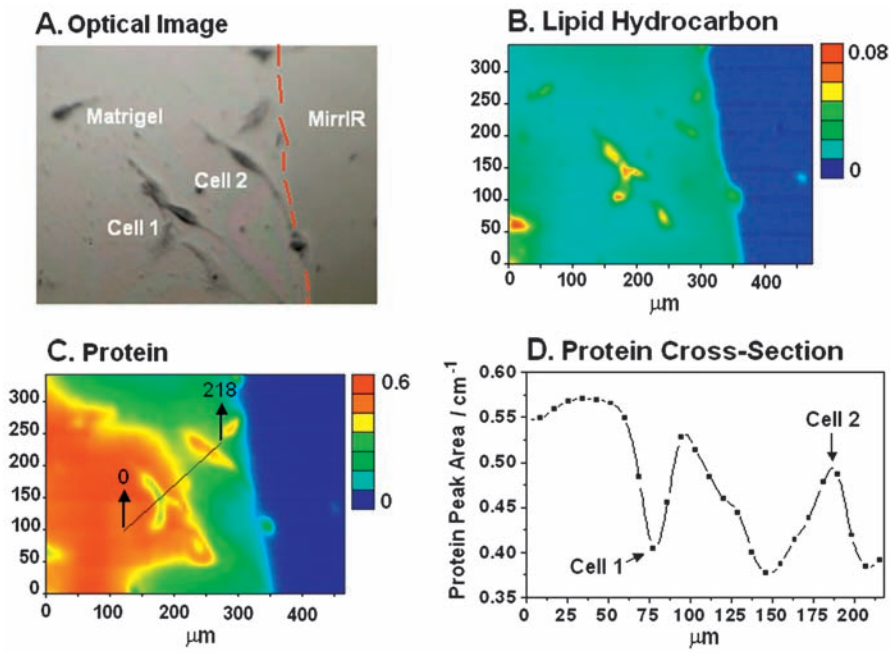

Figure 5.11 (A) Optical image of PC-3 cells on Matrigel. The red dotted line denotes the Matrigel (left)–MirrIR™ substrate (right) interface. FTIR spectral maps depicting the intensity distribution of the (B) lipid hydrocarbon and (C) protein peak area signals. (D) A cross-section through the protein intensity map is displayed as a graphical plot depicting the protein peak area values from a region of high concentration of Matrigel (at 0 μm) to one of lower concentration (towards 218 μm) and bisecting cells 1 and 2. (Reproduced from reference [65].)

AQ2

Local proteolysis of the Matrigel matrix was investigated using time-lapse video microscopy. The final frame of the time-lapse video and the brightfield image of the same area after fixation, relocated for FTIR-microspectroscopic imaging, are shown in Figures 5.12B (i) and (ii), respectively. These optical images demonstrate that the morphology of the cells (elongated and rounded), when in culture, is suitably retained by the formalin fixation procedure. In Figure 5.12A, the video frame captured at the start of the time-lapse recording shows that the cells at internal locations on Matrigel display a rounded morphology. The cell marked with a red arrowhead was stationary throughout the course of time-lapse recording and retained its rounded appearance. It is reasonable to assume that the low protein intensity at this cellular location [Figure 5.12B(iii)] would be indicative of local proteolysis or mechanical degradation of the Matrigel. However, between 5 h and the point of termination of the time-lapse study (22 h, 22 min), the cell marked with the green arrowhead migrated, several times, towards and away from the cells marked with the blue and white arrowheads. Since these cells (green, blue and

white arrowheads) were motile throughout the time-lapse recording, it is unlikely that there was local digestion of the Matrigel just prior to termination of the time-lapse recording *via* matrix metalloproteinases produced by the prostate cancer cells. Moreover, if proteolytic digestion was a dominant mechanism by which the green, blue and white arrowhead cells transversed the

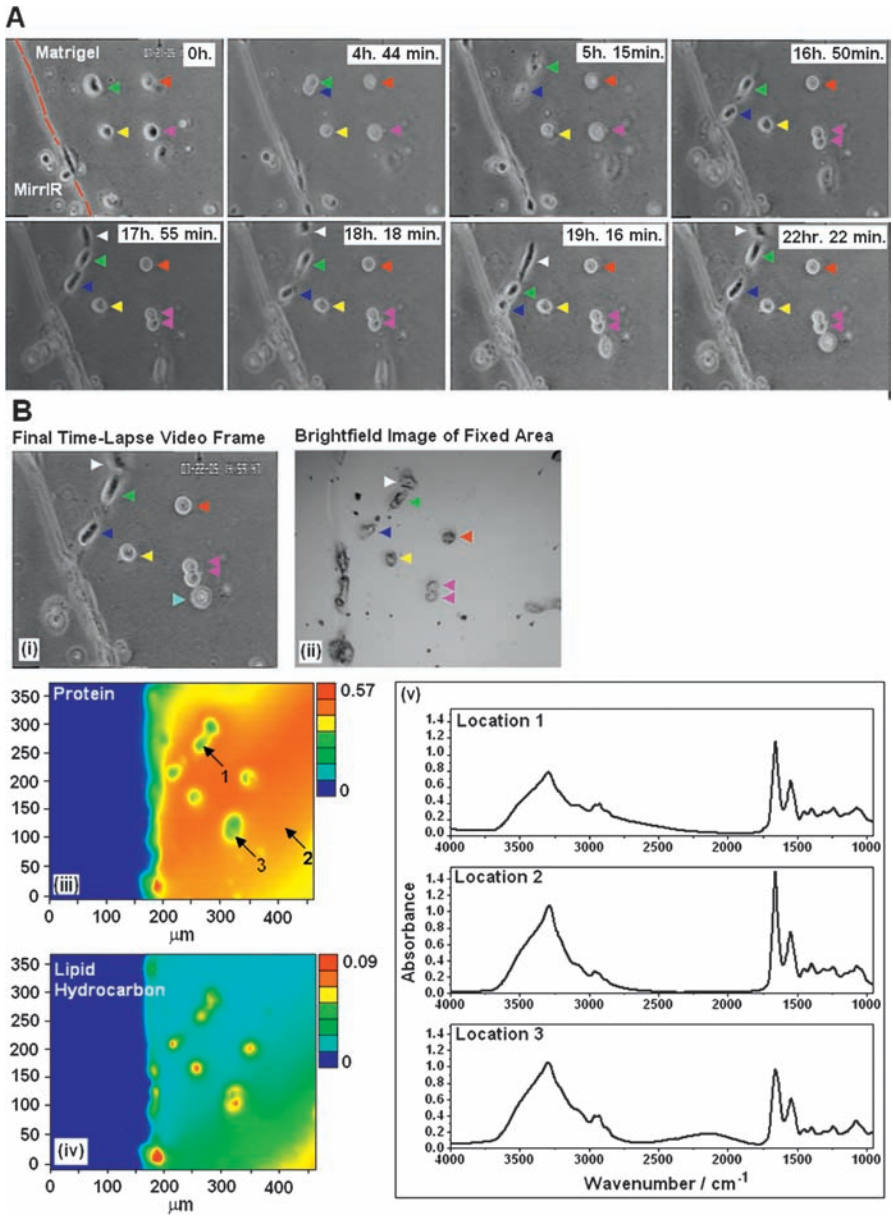

Matrigel, then one would expect low protein signals to arise from the entire path occupied by these cells. It was concluded from this, that light-scattering artefacts influenced the protein intensity maps of these cells on Matrigel, giving the illusion of protein degradation at the cell locations.[65]

A model was produced, which showed that a switch from a higher than background signal to a lower than background signal will occur at a given thickness or concentration of protein within the Matrigel layer. Importantly, the model includes light that is directly back-scattered into the microscope collection optics. These findings have a fundamental impact on research in the field of FTIR spectroscopy concerning cells on two-dimensional matrices.

5.3.5 Preparation of Living Cells for FTIR and Raman Studies

5.3.5.1 FTIR Studies

A number of studies concerning the analysis of living cells by FTIR have been performed with synchrotron radiation sources.[66–68] An early study by Holman *et al.* reported spectral changes in HepG2 cells (human hepatocellular carcinoma) treated with increasing doses of an environmental toxin.[66] In this study, post-treated cells were detached from culture substratum using trypsin, followed by two washes in PBS then kept as a suspension at 4 °C and measured with SR-FTIR within 24 h. Although the cool temperature minimizes the enzymatic effects of autolysis, without fixation there may be biochemical differences between cells at the zero time point compared with cells stored in PBS for 24 h, particularly for glycogen stores, since the cells were in a nutrient deficient environment. Nevertheless, it has been shown that spectra from these cells showed spectroscopic changes in the ratio of peak intensities ($1082\,cm^{-1}$/$1236\,cm^{-1}$) that could be correlated with increasing doses of toxin exposure. In a situation where the effect of time on cell biochemistry has not been assessed, one must be careful when associating spectral changes to the direct result of a condition administered to the cell. However, if spectral discrimination is achieved following randomized sampling of cells exposed to each of the

Figure 5.12 (A) Still frames taken from a time-lapse video of prostate cancer cells on Matrigel. The red dotted line at zero hours designates the Matrigel–MirrIR interface. Individual cells are labelled with coloured arrowheads for the ease of tracking cell migration across consecutive time frames and following figures. (B) Optical images of the (i) final frame of the time-lapse video (at 22 h, 22 min) and (ii) brightfield image of the same area, post fixation. Note that the image of the fixed area is rotated 22° compared with the image of the final frame such that the Matrigel–MirrIR interface is approximately vertical. The fixed area was analysed by FTIR microspectroscopy and the intensity distribution of the (iii) protein and (iv) lipid hydrocarbon domains are shown. (v) Representative raw IR spectra taken from three locations [1 and 3 (on cell) and 2 (on Matrigel)], from the protein intensity map, are also displayed. (Reproduced from reference [65].)

AQ2

different conditions, then this may evaluate whether live cell spectra are significantly influenced by their duration in nutrient deficient media.

More recently, specialized equipment for maintaining live T-1 cells (aneuploid cells from human kidney tissues) on gold-coated slides for *in-situ* SR-FTIR analysis has been investigated by Holman *et al.*[68] A mini-incubator system was used to sustain cell viability by maintaining a humidified environment, so as to retain a thin layer of growth medium around the cell during SR-FTIR measurements. The mini-incubator was temperature controlled at 37 °C *via* circulating water from a water bath, and IR transparent CaF_2 windows on the top cover were separately temperature controlled to avoid condensation. Using this incubator, the authors investigated any possible cytotoxic effects that may be elicited in the cell by exposure to the SR-IR radiation. Using the Alcian blue exclusion assay, it was found that the cells showed negative staining 24 h after exposure to 20 min of SR-IR radiation, which indicated that the cell membranes remained intact. The effects of 20 min SR-IR exposure on cell metabolism were assessed using the MTT assay. This confirmed that both control cells (not exposed to SR radiation) situated near to exposed cells and exposed cells produced mitochondrial dehydrogenases, which are associated with glycolysis and indicate negligible effects on this metabolic pathway. Finally, colony-forming assays demonstrated that there was no long-term damage as a result of SR-IR exposure.

Although these assays could not have been carried out *in situ* within the mini-incubator, it is encouraging to find that the length of time (20 min) that these cells were placed in the incubator had no short-term or long-term effects. Furthermore, the researchers reported that consecutive SR-FTIR spectra obtained at 10 min intervals for 30 min exhibited an unchanging IR spectrum to within 0.005 AU across the entire mid-IR spectral range. This provides supporting evidence for the justification of this experimental set-up for measuring single-point SR-FTIR spectra from single living cells. Since the experiment was carried out for only 30 min, changes in the spectrum over an extended time period, which is required to obtain cell maps, is unknown.

However, using a different experimental design for the sample compartment, Miljkovic *et al.* reported no spectral changes in spectra collected from live cells when data were collected every 30 min for 3 h.[69] Miljkovic *et al.* collected FTIR images at 6.25 μm × 6.25 μm pixel resolution of living HeLa cells (cervical cancer cell line) using the linear array detector Spotlight microspectrometer equipped with a glowbar source.[69] In this study, different approaches were used to prepare cells for transflection and transmission mode analysis. For transmission mode, live cells in growth medium were placed into a 6 μm pathlength CaF_2 liquid cell. This preparation resulted in the compression and rupturing of larger cells, however the smaller cells were left intact (Figure 5.13B). For transflection measurements, cells in buffered saline solution were placed as a drop onto a MirrIR slide and a CaF_2 or BaF_2 coverslip was placed on top. This preparation also involved the use of a 5 μm Teflon spacer to prevent the coverslip touching the MirrIR slide. Raw spectra obtained from FTIR images of HeLa cells using both modes of analysis showed an unusual Amide I to II ratio (Figure 5.13A and C),

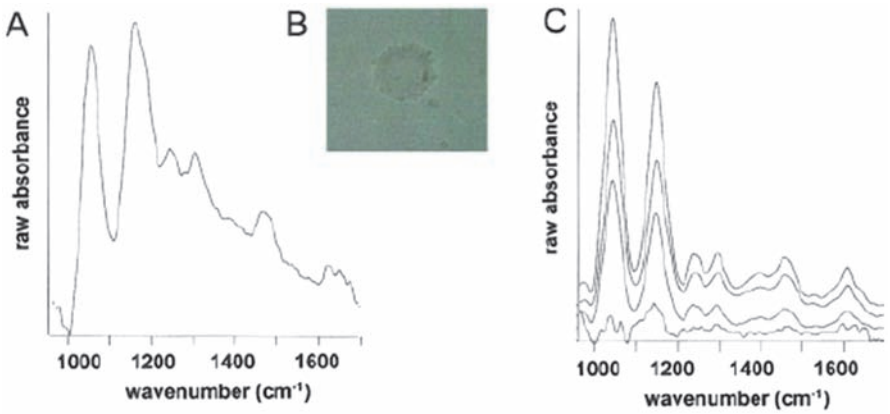

Figure 5.13 (A) Reflection/absorption spectrum and (B) visual image of a HeLa cell in BSS buffer, (C) Absorption spectra taken from a HeLa cell in growth medium. All spectra were collected with 128 scans at $4\,cm^{-1}$ spectral resolution. (Adapted from reference [69].)

AQ2

which was more apparent in transflection mode spectra (Figure 5.13A). This was attributed to the longer path length (10 μm) in the transflection mode measurement. The origin of this distorted Amide I to Amide II ratio was determined to be due to overcompensation of the water background from the cell spectrum, since the cell contains less water than the surrounding medium or buffer.

The authors suggested that correction of the Amide I and II peaks could be carried out by visually fitting a scaled buffer spectrum to the raw cell spectrum, until the resulting corrected spectrum shows a normal Amide A envelope. Although subjective, Miljkovic *et al.* demonstrated that it was possible to obtain a protein intensity image in which the HeLa cell displayed the expected high protein intensity, centered at its nucleus.[69]

In contrast to using cells in suspension as in the study by Miljkovic *et al.*,[69] cells used by Moss *et al.* were cultured directly onto CaF_2 plates.[67] This plate was placed into a liquid cell consisting of a 15 μm Teflon spacer, providing a pathlength of 11–12 μm and maintained at 35 °C. A constant flow of cell culture medium was passed through the cell at a rate of 230 μl/h. As in the study of Miljkovic *et al.*,[69] a background spectrum of growth medium was collected in a cell-free region of the sample and the ratios with the cell spectrum estimated. There was high reproducibility between SR-FTIR spectra obtained from 10 individual fibroblast cells when a spectrum of each cell was acquired every 24 min for 2 h. Although intrasampling differences were observed between cells, these were very much smaller than the standard deviation of repeated measurements for each cell. Moss *et al.* provide further support for the low spectral variance observed for live cell FTIR spectra, when collected within the first few hours of transfer to the sample analysis chamber.[67]

In agreement with the study by Miljkovic *et al.*,[69] a distorted Amide I to Amide II intensity ratio was observed by Moss *et al.*[67] However, since the

spectrum of background water is different from that of water bound to macromolecules, it was suggested that it is not possible to eliminate this background absorbance accurately. The authors also suggest that if the goal of the experiment is to obtain a spectrum from the same position of the exact same cell, before and after administration of a stimulus, then the difference between the spectra can be resolved even in the presence of background water. Additionally, it was found in this study that non-confluent cells could migrate out of the measuring SR beam. Moss *et al.* suggest that this could be minimized by placing the cell in a well.[67]

A recent study by Draux *et al.* investigated different optical substrates, quartz, calcium fluoride and zinc selenide, for preservation of cell integrity for Raman spectroscopy of single living cells.[70] Quartz was found to be the most appropriate based on cell morphology and proliferation rate.

5.3.5.2 Raman Studies

(See also Chapter 4, sections 4.7 and 4.8.) The spatial resolution of Raman spectroscopy is inherently higher than that of FTIR owing to the shorter wavelength of the excitation radiation (the diffraction limit is generally given as $\lambda/2$). An image obtained by Raman microspectroscopy requires raster scanning of a focused laser beam across the cell. Using this mode of data collection, an increase in spatial resolution, which is a function of step size and beam diameter, also increases the time for chemical mapping. Although in FTIR studies it has been shown that, for up to 3 h, spectral changes are not observed at the *whole-cell level* (see section 5.3.5.1), previously reported Raman maps of living cells have required ≥ 3 h collection times.[71] At the *subcellular level* one might expect that biochemical changes could occur within this period for a given sampling point. However, it has been shown that localization and spectral distinction between cytoplasmic and nuclear compartments in living cells was not affected in Raman maps of two different cell types (human osteogenic sarcoma cell and human embryonic lung epithelial fibroblast) that required long collection times (up to 20 h).[71] In this study by Krafft *et al.*,[71] difference spectra of the cytoplasm and nucleus identified the important discriminatory variables that distinguished these compartments: nucleic acids and lipids. In fact, analysis of living cells grown on quartz and analysed in media provided Raman spectra containing features of subcellular components that were more pronounced than those obtained from frozen-hydrated cells. This was attributed to conformational changes and aggregation of biomolecular constituents caused by the freeze-drying process and which are not present when the cells are analysed hydrated.

The acquisition time for a Raman map of a cell can be improved by increasing the sensitivity of the technique. Kneipp *et al.* have demonstrated that enhanced Raman signals (10–14 orders of magnitude) for the native constituents of a cell can be achieved by incorporating colloidal gold particles into the cell.[72,73] The gold nanoparticles give rise to surface-enhanced Raman

scattering (SERS) where Raman molecules close to the vicinity of the nanoparticles experience electronic interaction with enhanced optical fields due to resonances of the applied optical fields with the surface plasmon oscillations of the metallic nanostructures. This process results in an increase in the scattering cross-section of the Raman molecules, which enabled Raman maps to be collected at 1 μm lateral resolution (1 s for one mapping point)[72] where each spectrum in the map consisted of the spectral region 400–1800 cm^{-1}.

Delivery of the nanoparticles into the cell interior can be carried out in two ways, sonication or fluid-phase uptake.[72] The fluid-phase uptake method involves supplementing the culture medium with colloidal gold suspensions (60 nm in size), 24 h prior to experiments. The cells internalize the nanoparticles through endocytosis and without further induction (Figure 5.14A).[73] This can result in the formation of colloidal aggregates inside the cell that may be 100 nm to a few micrometers in size.[72] The cells are washed in buffer to remove non-incorporated nanoparticles and replaced in fresh buffer for SERS analysis. The second method of delivering nanoparticles into the cell is by sonication, where rupture of the cell membrane enables an influx of nanoparticles before self-annealing within a few seconds. However, in low-intensity ultrasound mediated gene transfection, it has been found that sonication can induce stress responses in the cell,[74] and so it should be carried out 24 h prior to experiment to allow enough time for the cell to repair any damage. Incorporation of the nanoparticles into the cell using the fluid-phase uptake method was not found to yield any visible changes in growth characteristics such as signs of apoptosis or cell detachment when compared to a control cell culture.[72] Raman spectra obtained from different locations in the nanoparticle doped cell gave rise to very different spectral profiles, illustrating the biochemical heterogeneity of the cell (Figure 5.14B).

Another signal enhancement technique, CARS (coherent anti-Stokes Raman spectroscopy) uses multiple lasers to excite coherent anti-Stokes Raman scattering. CARS microscopy is a rapid vibrational imaging technique and has been used to image mitosis and apoptosis in living cells,[75] for real-time visualization of organelle transport in living cells,[76] and for quantitative imaging of intracellular lipid droplets.[77] Stimulated Raman scattering, which has a significantly greater sensitivity than spontaneous Raman scattering, has been used to monitor the uptake of omega-3 fatty acids by living human lung cancer cells.[78] No plasma membrane blebbing was observed following repeated imaging of the same cells indicating that no photodamage had occurred.

As well as the application of Raman microspectroscopy to live cell imaging, the technique has also been applied for the phenotypic typing of live cells. Krishna and colleagues collected Raman spectra of two different cell lines and their respective drug resistant analogues: breast cancer cell line MCF7 and its subclone resistant to verapamil (MCF7/VP) and promyelocytic leukaemia HL60S cell line and its multidrug-resistant phenotypes (HL60/DOX: resistant to doxorubicin; HL60/DNR: resistant to daunorubicin).[58] PCA analyses of these Raman spectra were able to generate score plots that showed clustering and separation for each cell line and its drug-resistant clone. The authors also

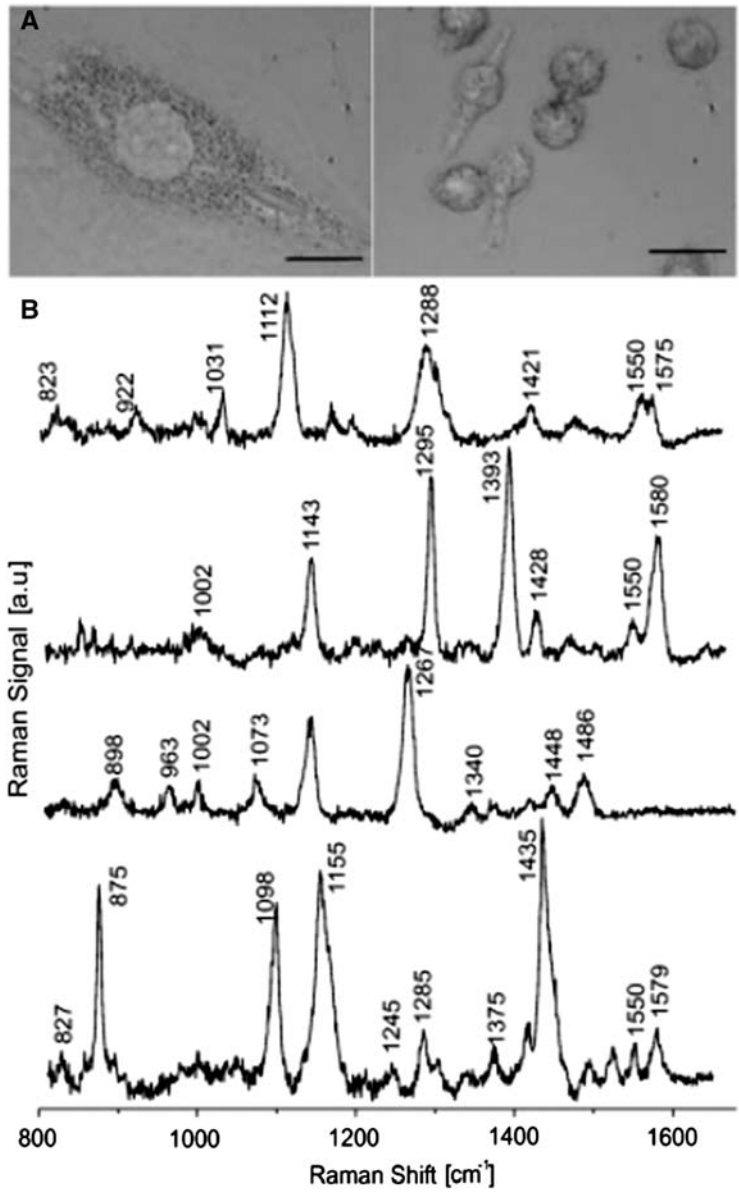

Figure 5.14 (A) Cells of a fibroblast cell line, NIH/3T3 (nonphagocytic) (left), and a macrophage cell line, J774 (phagocytic) (right), after uptake of gold nanoparticles; particle accumulations are visible as black dots inside the cells. Scale bars 20 μm. (B) Examples of SERS spectra acquired from NIH/3T3 cells after 3 h incubation with gold nanostructures, excitation wavelength 830 nm, 1 s collection time. (Reproduced from reference [73].)

AQ2

carried out these experiments using FTIR and found that classification, discrimination and reproducibility were greater using this method. However, with the view of translating this type of analysis to clinical application, it would be desirable for the chosen method to incorporate minimal sample preparation for high-throughput screening. For the Raman study, a cell pellet consisting of 1×10^6 cells (washed in 0.9% NaCl) was used directly for spectroscopic analysis, whereas for the FTIR experiments a time-limiting step was required that consisted of drying a cell suspension under mild vacuum onto a zinc selenide sample wheel.

The sample preparation method used by Krishna *et al*. for the Raman study requires fast data acquisition times, since live cell pellets surrounded by a thin layer of aqueous buffer may undergo biochemical changes over-time.[58] In their study, 25 spectra were collected for each pellet, where one spectrum took 4.5 min to collect. Thus, between the first and final spectrum there was a time-lag of 1 h and 53 min. If biochemical changes did occur during this period, then it may have contributed to the lower discriminatory power achieved using Raman spectra in this study. In contrast, the FTIR spectra were obtained from dried cells, providing perhaps a background interference that is constant over all cells and so differences due to MDR or drug sensitive phenotypes could be more readily resolved. This provides further evidence that possible artefacts from the drying process do not hamper spectroscopic differentiation between cells of differing phenotypes (as mentioned in section 5.3.2).

More recent phenotyping studies by Chan *et al*.[79–81] and Harvey *et al*.[82] have used Laser Tweezers Raman Spectroscopy (LTRS) to optically trap single living cells suspended in PBS.

5.4 Conclusions

Sample preparation is a key aspect of any experimental design and particularly so for spectroscopic analysis of cells and tissues. The continuing developments in tissue preservation for optimum detection of specific biomolecules using emerging bioanalytical approaches will shape the tissue repositories of the future. These developments will also have an impact on biomedical vibrational spectroscopy, since this technology can play an important role in determining the biochemical basis underpinning disease progression. Nevertheless, it is apparent that existing tissue banks have proven adequate for FTIR and Raman studies of tissue pathologies, providing high classification power. This is despite the fact that spectral artefacts exist as a result of sample processing. These spectral artefacts can be due to protein depolymerization or a change in the lipid to protein ratio for dried cryosections, or in the case of deparaffinized sections, due to residual paraffin, coagulation of proteins and loss of lipids.

As discussed in section 5.2, some of these artefacts can be minimized. Protein depolymerization of freeze-dried/thawed cryosections can be reduced by careful attention to the cryogen used for initial tissue snap-freezing as well as cryomicrotomy and freeze-drying environmental temperatures. Other artefacts such

as residual paraffin can now be confidently removed in the light of work carried out by Faoláin *et al.*[28] It appears that deparaffinization using hexane for >20 h is an appropriate method for this purpose and this has wider implications in immunohistochemical pathology. However, this protocol can be time limiting and so less rigorous protocols may be sufficient where spectroscopic markers for pathological assessment do not overlap with paraffin signals.[30,31]

The early work of Fox *et al.*,[25] investigating the binding time of formalin to tissue, may be of significance to those vibrational spectroscopists presently using formalin fixed cells in imaging or biomechanistic studies, since the effects of formalin binding time on cell spectra have not been assessed. Although cell line dependent, formalin fixation has been shown to provide cell preservation similar to the live cell state.[52]

Tailored chemical fixation protocols for vibrational spectroscopy may however be necessary in some instances. For example, as described in section 5.3.2, the lipid component of adipocytes requires fixation with OsO_4.[53] Coupled to paraformaldehyde, a well-preserved sample can be obtained for spectroscopic analysis. The lengthy procedure of OsO_4–paraformaldehyde with CPD is appropriate where experiments are capturing a cellular event at time-frames that are far apart. However, for shorter time frames (intervals of 15 min), faster fixation methods are required and formalin has so far been proven to be adequate.[54] Interestingly, it has also been demonstrated that air-dried cells following exposure to a pharmacological drug or stimulus can also produce spectral changes that may be associated with response to the condition administered.[55]

There have been encouraging results reported within the context of live cell experiments using FTIR. The collective demonstration of biochemical stability for different cell types (T-1, HeLa and fibroblasts) by the various research groups working within this field,[67–69] together with the suggestion of Moss *et al.*[67] that correction for water absorbance may not be necessary, suggests that future FTIR studies may be able to measure early biochemical responses of single living cells to stimuli. Raman based live cell studies have shown excellent prospects for cell phenotyping as well as probing the distributions of native biomolecules of a cell with high sensitivity and spatial resolution and without the requirement for exogenous labelling.

In summary, for spectroscopic analysis of tissue samples, fresh or carefully prepared frozen tissue would be considered ideal, but FFPP tissue can be used successfully if deparaffinized using hexane. Other dewaxing agents and protocols can also be used successfully if the paraffin signals do not overlap with the spectral regions of interest. For analysis of cell samples, live cells would be considered ideal, but in cases where this is not possible or practical, fixed cells can be used. Formalin has been shown to provide good cellular preservation for spectroscopic analysis in many studies but some experimentation may be necessary to find the optimum fixative for each particular cell sample. For this optimization, fixed cell samples should be compared with live cell samples where possible.

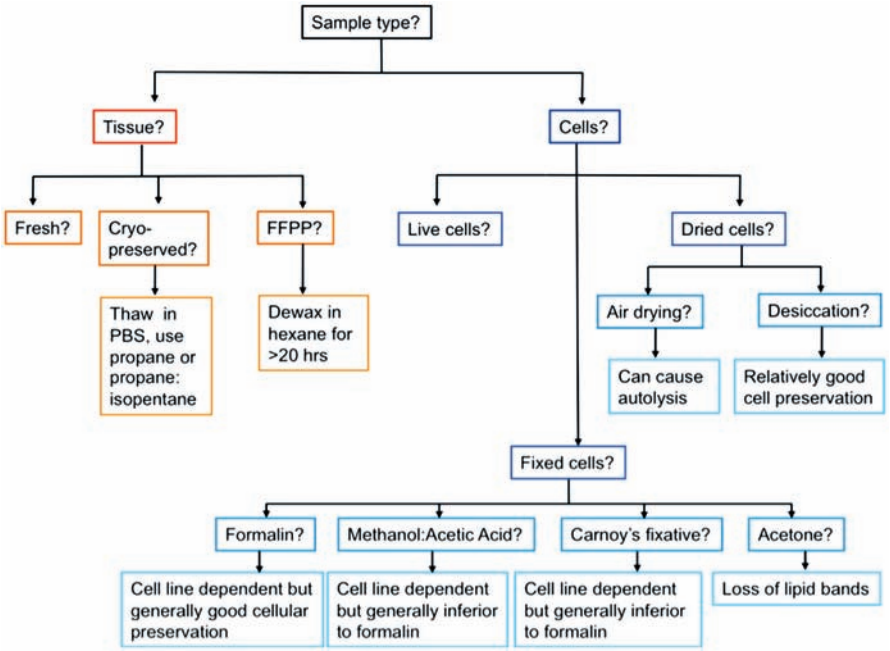

Figure 5.15 Sample preparation choices for tissues and cells.

Figure 5.15 provides an overview of common sample preparation choices for tissue and cell samples together with some recommendations based on the studies discussed in this chapter.

Acknowledgements

Support was received from the Association for International Cancer Research (AICR Grant number 04-518), The Prostate Cancer Foundation (PG and EG) and from the NBIPI programme, funded by the Irish Government's Programme for Research in Third Level Institutions, Cycle 4, National Development Plan 2007–2013, supported by the European Union Structural Fund and the Technology Sector Research (Strand 3) programme of the Irish Higher Education Authority (FL) during the writing of this article and some of the experiments described within it. We are grateful to Dr Stephen Murray (Paterson Institute for Cancer Research, UK) for use of the time-lapse video microscope.

References

1. J. A. Kiernan, Formaldehyde, formalin, paraformaldehyde and glutaraldehyde: What they are and what they do, *Microsc. Today*, 2000, **00–1**, 8–12.

2. D. Jones, *Introduction*, In: *Fixation in Histochemistry*, P. J. Stoward, (eds). Chapman and Hall, London, 1973, 2–7.
3. G. R. Turbett and L. N. Sellner, The use of optimal cutting temperature compound can inhibit amplification by polymerase chain reaction, *Diagn. Molec. Pathol.*, 1997, **6**, 298–303.
4. J. W. Gillespie, Evaluation of Non-Formalin Tissue Fixation for Molecular Profiling Studies, *Am. J. Pathol.*, 2002, **160**, 449–457.
5. P. G. L. Andrus and R. D. Strickland, Cancer grading by Fourier Transform Infrared Spectroscopy, *Biospectroscopy*, 1998, **4**, 37–46.
6. S. Takahashi, A. Satomi, K. Yano, H. Kawase, T. Tanimizu, Y. Tuji, S. Murakami and R. Hirayama, Estimation of glycogen levels in human colorectal cancer tissue: relationship with cell cycle and tumour outgrowth, *J. Gastroenterol.*, 1999, **34**, 474–480.
7. D. C. Fernandez, R. Bhargava, S. M. Hewitt and I. W. Levin, Infrared spectroscopic imaging for histopathological recognition, *Nature Biotechnol.*, 2005, **23**, 469–474.
8. M. G. Shim and B. C. Wilson, The effects of ex vivo handling procedures on the near-infrared Raman spectra if normal mammalian tissues, *Photochem. Photobiol.*, 1996, **63**, 662–671.
9. E. O. Faoláin, M. B. Hunter, J. M. Byrne, P. Kelehan, M. McNamara, H. J. Byrne and F. M. Lyng, A study examining the effects of tissue processing on human tissue sections using vibrational spectroscopy, *Vib. Spectrosc.*, 2005, **38**(1–2), 121–127.
10. Z. W. Huang, A. McWilliams, S. Lam, J. English, D. I. McLean, H. Lui and H. Zeng, Effect of formalin fixation on the near-infrared Raman spectroscopy of normal and cancerous human bronchial tissues, *Int. J. Oncol.*, 2003, **23**, 649–655.
11. N. L. Pleshko, A. L. Boskey and R. Mendelsohn, An FT-IR microscopic investigation of the effects of tissue preservation on bone, *Calcif. Tissue Int.*, 1992, **51**, 72–77.
12. J. L. Stephenson, Ice crystal growth during the rapid freezing of tissues, *J. Biophys. Biochem. Cytol.*, 1956, **2**, 45–52.
13. N. Stone, C. Kendall, J. Smith, P. Crow and H. Barr, Raman spectroscopy for identification of epithelial cancers, *Faraday Discuss.*, 2003, **126**, 141–157.
14. N. Stone, M. C. H. Prieto, P. Crow, J. Uff and A. W. Ritchie, The use of Raman spectroscopy to provide an estimation of the gross biochemistry associated with urological pathologies, *Anal. Bioanal. Chem.*, 2007, **387**, 1657–1668.
15. H. Wills, R. Kast, C. Stewart, R. Rabah, A. Pandya, J. Poulik, G. Auner and M. D. Klein, Raman spectroscopy detects and distinguishes neuroblastoma and related tissues in fresh and (banked) frozen specimens, *J. Pediatr. Surg.*, 2009, **44**, 386–391.
16. M. Jackson, J. R. Mansfield, B. Dolenko, R. L. Somorjai, H. H. Mantsch and P. H. Watson, Classification of breast tumours by grade and steroid

receptor status using pattern recognition analysis of infrared spectra, *Cancer Detect. Prevent.*, 1999, **23**, 245–253.
17. M. Meurens, J. Wallon, J. Tong, H. Noel and J. Haot, Breast cancer detection by Fourier transform infrared spectrometry, *Vib. Spectrosc.*, 1996, **10**, 341–346.
18. G. Muller, W. Wasche, U. Bindig and K. Liebold, IR-Spectroscopy for tissue differentiation in the medical field, *Laser Phys.*, 1999, **9**, 348–356.
19. R. Wiens, M. Rak, N. Cox, S. Abraham, B. H. J. Juurlink, W. M. Kulyk and K. M. Gough, Synchrotron FTIR microspectroscopic analysis of the effects of anti-inflammatory therapeutics on wound healing in laminectomized rats, *Anal. Bioanal. Chem.*, 2007, **387**, 1679–1689.
20. C. P. Schultz, The potential role of Fourier transform infrared spectroscopy and imaging in cancer diagnosis incorporating complex mathematical methods, *Technol. Cancer Res. Treat.*, 2002, **1**, 95–104.
21. C. Beleites, G. Steiner, M. G. Sowa, R. Baumgartner, S. Sobottka, G. Schackert and R. Salzer, Classification of human gliomas by infrared imaging spectroscopy and chemometric image processing, *Vib. Spectrosc.*, 2005, **38**, 143–149.
22. P. B. Medawar, The rate of penetration of fixatives, *J. Roy. Microsc. Soc.*, 1941, **61**, 46.
23. C. H. Fox, F. B. Johnson, J. Whiting and P. P. Roller, Formaldehyde fixation, *J. Histochem. and Cytochem.*, 1985, **33**, 845–853.
24. T. J. Mason and T. J. O'Leary, Effects of formaldehyde fixation on protein secondary structure: a calorimetric and infrared spectroscopic investigation, *J. Histochem. Cytochem.*, 1991, **39**, 225–229.
25. S. Aparicio, S. B. Doty, N. P. Camacho, E. P. Paschalis, L. Spevak, R. Mendelsohn and A. L. Boskey, Optimal methods for processing mineralized tissues for Fourier transform infrared microspectroscopy, *Calcif. Tissue Int.*, 2002, **70**, 422–429.
26. Y. N. Yeni, J. Yerramshetty, O. Akkus, C. Pechey and C. M. Les, Effect of Fixation and Embedding on Raman Spectroscopic Analysis of Bone Tissue, *Calcif. Tissue Int.*, 2006, **78**, 363–371.
27. R. K. Sahu, S. Argov, A. Salman, U. Zelig, M. Huleihel, N. Grossman, J. Gopas, J. Kapelushnik and S. Mordechai, Can Fourier transform infrared spectroscopy at higher wavenumbers (mid IR) shed light on biomarkers?, *J. Biomed. Opt.*, 2005, **10**, 05017–05027.
28. E. O. Faolain, M. B. Hunter, J. M. Byrne, P. Kelehan, H. A. Lambkin, H. J. Byrne and F. M. Lyng, Raman spectroscopic evaluation of efficacy of current paraffin wax section dewaxing agents, *J. Histochem. Cytochem.*, 2005, **53**, 121–129.
29. K. Poon, I. Lydon, H. Lambkin, N. Rashid, H. J. Byrne, F. M. Lyng, Investigation of dewaxing agents and protocols on formalin-fixed paraffin-embedded tissues by Raman spectroscopy, *Manuscript in preparation.*
30. E. Gazi, M. Baker, J. Dwyer, N. P. Lockyer, P. Gardner, J. H. Shanks, R. S. Reeve, C. A. Hart, M. D. Brown and N. W. Clarke, A Correlation of

FTIR Spectra Derived From Prostate Cancer Tissue with Gleason Grade and Tumour Stage, *Eur. Urol.*, 2006, **50**, 750–761.
31. E. Gazi, J. Dwyer, P. Gardner, A. Ghanbari-Siahkali, A. Wade, J. Miyan, N. P. Lockyer, J. C. Vickerman, N. W. Clarke, J. H. Shanks, L. J. Scott, C. Hart and M. Brown, Applications of FTIR -Microspectroscopy to Benign Prostate and Prostate Cancer, *J. Pathol.*, 2003, **201**, 99–108.
32. C. W. Meuse and P. E. Barker, Quantitative Infrared Spectroscopy of Formalin-fixed, Paraffin-embedded Tissue Specimens, Paraffin Wax Removal With Organic Solvents, *Appl. Immunohistochem. Mol. Morphol.*, 2009, **17**(6), 547–52.
33. A. Tfayli, O. Piot, A. Durlach, P. Bernard and M. Manfait, Discriminating nevus and melanoma on paraffin-embedded skin biopsies using FTIR microspectroscopy, *Biochim. Biophys. Acta.*, 2005, **1724**, 262–269.
34. A. Tfayli, C. Gobinet, V. Vrabie, R. Huez, M. Manfait and O. Piot, Digital Dewaxing of Raman Signals: Discrimination Between Nevi and Melanoma Spectra Obtained from Paraffin-Embedded Skin Biopsies, *Appl. Spectrosc.*, 2009, **63**(5), 564–70.
35. C. Gobinet, V. Vrabie, A. Tfayli, O. Piot, R. Huez and M. Manfait, Preprocessing and source separation methods for Raman spectra analysis of biomedical samples, *Conf. Proc. IEEE Eng. Med. Biol. Soc.*, 2007, 6208–11.
36. E. Ly, O. Piot, R. Wolthuis, A. Durlach, P. Bernard and M. Manfait, Combination of FTIR spectral imaging and chemometrics for tumour detection from paraffin-embedded biopsies, *Analyst*, 2008, **133**, 197–205.
37. E. Ly, O. Piot, A. Durlach, P. Bernard and M. Manfait, Differential diagnosis of cutaneous carcinomas by infrared spectral micro-imaging combined with pattern recognition, *Analyst*, 2009, **134**, 1208–1214.
38. V. Untereiner, O. Piot, M. D. Diebold, O. Bouché, E. Scaglia and M. Manfait, Optical diagnosis of peritoneal metastases by infrared microscopic imaging, *Anal. Bioanal. Chem.*, 2009, **393**, 1619–1627.
39. L. Chiriboga, P. Xie, H. Yee, V. Vigorita, D. Zarou, D. Zakim and M. Diem, Infrared spectroscopy of human tissue. I. Differentiation and Maturation of epithelial cells in the human cervix, *Biospectroscopy*, 1998, **4**, 47–53.
40. H. Y. N. Holman, M. C. Martin, E. A. Blakely, K. Bjornstad and W. R. McKinney, IR spectroscopic characteristics of a cell cycle and cell death probed by synchrotron radiation based Fourier transform IR spectromicroscopy, *Biopolymers (Biospectroscopy)*, 2000, **57**, 329–335.
41. P. Lasch, M. Boese, A. Pacifico and M. Diem, FT-IR spectroscopic investigations of single cells on the subcellular level, *Vib. Spectrosc.*, 2002, **28**, 147–157.
42. P. Lasch, A. Pacifico and M. Diem, Spatially resolved IR microspectroscopy of single cells, *Biopolymers (Biospectroscopy)*, 2002, **67**, 335–338.
43. D. Yang, D. J. Castro, I. E. El-Sayed, M. A. El-Sayed, R. E. Saxton and N. Y. Zhang, A Fourier-transform infrared spectroscopic comparison of cultured human fibroblast and fibrosacroma cells: A new method for detection of malignancies, *J. Clin. Laser Med. Surg.*, 1995, **13**, 55–59.

44. A. Salman, J. Ramesh, V. Erukhimovitch, M. Talyshinksy, S. Mordechai and M. Huleihel, FTIR microspectroscopy of malignant fibroblasts transformed by mouse sarcoma virus, *J. Biochem. Biophys. Meth.*, 2003, **55**, 141–153.
45. M. J. Tobin, M. A. Chesters, J. M. Chalmers, F. J. M. Rutten, S. E. Fisher, I. M. Symonds, A. Hitchcock, R. Allibone and S. Dias-Gunasekara, Infrared microscopy of epithelial cancer cells in whole tissues and in tissue culture, using synchrotron radiation, *Faraday Discuss.*, 2004, **126**, 27–38.
46. H. P. Wang, H. C. Wang and Y. J. Huang, Microscopic FTIR studies of lung cancer cells in pleural fluid, *Sci. Total Environ.*, 1997, **204**, 283–287.
47. N. Jamin, P. Dumas, J. Moncutt, W.-H. Fridman, J.-L. Teillaud, G. L. Carr and G. P. Williams, Highly resolved chemical imaging of living cells by using synchrotron infrared microspectrometry, *Proc. Natl. Acad. Sci. USA*, 1998, **95**, 4837–4840.
48. E. Gazi, J. Dwyer, N. P. Lockyer, P. Gardner, J. Miyan, C. A. Hart, M. D. Brown and N. W. Clarke, Fixation Protocols for subcellular imaging using synchrotron based FTIR-microspectroscopy, *Biopolymers*, 2005, **77**, 18–30.
49. J. A. Kieran, *Chapter 2 Fixation*, In: *Histological and Histochemical Methods: Theory & Practice*, Pergamon Press, Oxford, UK, 1990, 10–35.
50. T. J. Harvey, C. Hughes, A. D. Ward, E. C. Faria, A. Henderson, N. W. Clarke, M. D. Brown, R. D. Snook and P. Gardner, Classification of fixed urological cells using Raman tweezers, *J. Biophoton.*, 2009, **2**(1–2), 47–69.
51. M. M. Mariani, P. Lampen, J. Popp, B. R. Wood and V. Deckert, Impact of fixation on in vitro cell culture lines monitored with Raman spectroscopy, *Analyst.*, 2009, **134**(6), 1154–61.
52. A. D. Meade, C. Clarke, F. Draux, G. D. Sockalingum, M. Manfait, F. M. Lyng, H. J. Byrne, Studies of chemical fixation effects in human cell lines using Raman microspectroscopy, *Anal. Bioanal. Chem.*, Epub, Jan 20, 2010.
53. E. Gazi, P. Gardner, N. P. Lockyer, C. A. Hart, N. W. Clarke and M. D. Brown, Probing Lipid Translocation Between Adipocytes and Prostate Cancer Cells with Imaging FTIR Microspectroscopy, *J. Lipid Res.*, 2007, **48**, 1846–1856.
54. E. Gazi, T. J. Harvey, P. Gardner, N. P. Lockyer, C. A. Hart, N. W. Clarke and M. D. Brown, A FTIR Microspectroscopic Study of the Uptake and Metabolism of Isotopically Labelled Fatty Acids by Metastatic Prostate Cancer, *Vib. Spectrosc.*, 2009, **50**, 99–105.
55. J. Sule-Suso, D. Skingsley, G. D. Sockalingum, A. Kohler, G. Kegelaer, M. Manfait and A. J. El Haj, FT-IR microspectroscopy as a tool to assess lung cancer cells response to chemotherapy, *Vib. Spectrosc.*, 2005, **38**, 179–184.
56. P. Crow, B. Barrass, C. Kendell, M. Hart-Prieto, M. Wright, R. Persad and M. Stone, The use of Raman spectroscopy to differentiate between different prostatic adenocarcinoma cell lines, *Br. J. Cancer*, 2005, **92**, 2166–2170.

57. C. M. Krishna, G. D. Sockalingum, G. Kegelaer, S. Rubin, V. B. Kartha and M. Manfait, Micro-Raman spectroscopy of mixed cancer cell populations, *Vib. Spectrosc.*, 2005, **38**, 95–100.
58. M. C. Krishna, G. Kegelaer, I. Adt, S. Rubin, V. B. Kartha, M. Manfait and G. D. Sockalingum, Characterisation of uterine sarcoma cell lines exhibiting MDR phenotype by vibrational spectroscopy, *Biochim. Biophys. Acta*, 2005, **1726**, 160–167.
59. E. Gazi, J. Dwyer, P. Gardner, A. Ghanbari-Siahkali, A. Wade, J. Miyan, N. P. Lockyer, J. C. Vickerman, N. W. Clarke, J. H. Shanks, L. J. Scott, C. Hart and M. Brown, Applications of FTIR-Microspectroscopy to Benign Prostate and Prostate Cancer, *J. Pathol.*, 2003, **201**, 99–108.
60. T. J. Harvey, E. Gazi, N. W. Clarke, M. D. Brown, E. C. Faria, R. D. Snook and P. Gardner, Discrimination of Prostate Cancer Cells by FTIR Photo-Acoustic Spectroscopy, *Analyst.*, 2007, **132**, 292–295.
61. T. J. Harvey, E. Gazi, A. Henderson, R. D. Snook, N. W. Clarke, M. Brown and P. Gardner, Factors influencing the Discrimination and Classification of Prostate Cancer Cell Lines by FTIR Microspectroscopy, *Analyst*, 2009, **134**, 1083–1091.
62. S. Z. Haslam and T. L. Woodward, Host microenvironment in breast cancer development: Epithelial-cell–stromal-cell interactions and steroid hormone action in normal and cancerous mammary gland, *Breast Cancer Res.*, 2003, **5**, 208–215.
63. C. Krafft, R. Salzer, S. Seitz, C. Ern and M. Schieker, Differentiation of individual human mesenchymal stem cells probed FTIR microscopic imaging, *Analyst*, 2007, **132**, 647–653.
64. A. D. Meade, F. M. Lyng, P. Knief and H. J. Byrne, Growth substrate induced functional changes elucidated by FTIR and Raman spectroscopy in in-vitro cultured human keratinocytes, *Anal. Bioanal. Chem.*, 2007, **387**, 1717–1728.
65. J. Lee, E. Gazi, J. Dwyer, N. P. Lockyer, M. D. Brown, N. W. Clarke and P. Gardner, Optical Artifacts in Transflection Mode FTIR Microspectroscopic Images of Single Cells on a Biological Support: Does Rayleigh Scattering Play a Role?, *Analyst*, 2007, **132**, 750–755.
66. H.-Y. N. Holman, R. Goth-Goldstein, M. C. Martin, M. L. Russell and W. R. McKinney, Low-dose responses to 2,3,7,8-tetrachlorodibenzo-*p*-dioxin in single living human cells measured by synchrotron infrared spectromicroscopy, *Environ. Sci. Technol.*, 2000, **34**, 2513–2517.
67. D. Moss, M. Keese and R. Pepperkok, IR microspectroscopy of live cells, *Vib. Spectrosc.*, 2005, **38**, 185–191.
68. H. Y. N. Holman, M. C. Martin and W. R. McKinney, Synchrotron-based FTIR spectromicroscopy: Cytotoxicity and heating considerations, *J. Biomed. Phys.*, 2003, **29**, 275–286.
69. M. Miljkovic, M. Romeo, C. Matthaus and M. Diem, Infrared microspectroscopy of individual human cervical cancer (HeLa) cells suspended in growth medium, *Biopolymers*, 2004, **74**, 172–175.

70. F. Draux, P. Jeannesson, A. Beljebbar, A. Tfayli, N. Fourre, M. Manfait, J. Sulé-Suso and G. D. Sockalingum, Raman spectral imaging of single living cancer cells: a preliminary study, *Analyst*, 2009, **134**(3), 542–8.
71. C. Krafft, T. Knetschke, A. Siegner, R. H. W. Funk and R. Salzer, Mapping of single cells by near infrared Raman microspectroscopy, *Vib. Spectrosc.*, 2003, **32**, 75–83.
72. K. Kneipp, A. S. Haka, H. Kneipp, K. Badizadegan, N. Yoshizawa, C. Boone, K. E. Shafer-Peltier, J. T. Motz, R. R. Dasari and M. S. Feld, Surface-enhanced Raman spectroscopy in single living cells using gold nanoparticles, *Appl. Spectrosc.*, 2002, **56**, 150–154.
73. K. Kneipp, H. Kneipp and H. Kneipp, Surface-enhanced Raman scattering in local optical fields of silver and gold nanoaggregates – From single-molecule Raman spectroscopy to ultrasenstive probing in live cells, *Acc. Chem. Res.*, 2006, **39**, 443–450.
74. L. B. Feril, T. Kondo, Y. Tabuchi, R. Ogawa, Q.-L. Zhao, T. Nozaki, T. Yoshida, N. Kudo and K. Tachibana, Biomolecular effects of low-intensity ultrasound: apoptosis, sonotransfection, and gene expression, *Japan. J. Appl. Phys.*, 2007, **46**, 4435–4440.
75. J. X. Cheng, Y. K. Jia, G. Zheng and X. S. Xie, Laser-scanning coherent anti-Stokes Raman scattering microscopy and applications to cell biology, *Biophys. J.*, 2002, **83**, 502–509.
76. X. Nan, E. O. Potma and X. S. Xie, Nonperturbative chemical imaging of organelle transport in living cells with coherent anti-stokes Raman scattering microscopy, *Biophys J.*, 2006, **91**(2), 728–35.
77. H. Rinia, K. N. Burger, M. Bonn and M. Muller, Quantitative label-free imaging of lipid composition and packing of individual cellular lipid droplets using multiplex CARS microscopy, *Biophys. J.*, 2008, **95**, 4908–4914.
78. C. W. Freudiger, W. Min, B. G. Saar, S. Lu, G. R. Holtom, C. He, J. C. Tsai, J. X. Kang and X. S. Xie, Label-free biomedical imaging with high sensitivity by stimulated Raman scattering microscopy, *Science*, 2008, **322**(5909), 1857–61.
79. J. W. Chan, D. S. Taylor, T. Zwerdling, S. M. Lane, K. Ihara and T. Huser, Micro-Raman spectroscopy detects individual neoplastic and normal hematopoietic cells, *Biophys. J.*, 2006, **90**(2), 648–56.
80. J. W. Chan, D. S. Taylor, S. M. Lane, T. Zwerdling, J. Tuscano and T. Huser, Nondestructive identification of individual leukemia cells by laser trapping Raman spectroscopy, *Anal. Chem.*, 2008, **80**(6), 2180–7.
81. J. W. Chan and D. K. Lieu, Label-free biochemical characterization of stem cells using vibrational spectroscopy, *J. Biophoton.*, 2009, **2**(11), 656–68.
82. T. J. Harvey, E. Correia Faria, E. Gazi, A. D. Ward, N. W. Clarke, M. D. Brown, R. D. Snook and P. Gardner, The Spectral Discrimination of Live Prostate and Bladder Cancer Cell Lines Using Raman Optical Tweezers, *J. Biomed. Opt.*, 2008, **13**, 064004.